

Galaxy clusters in the Perseus–Pisces region – I. Spectroscopic and photometric data for early-type galaxies

R.J. Smith¹, J.R. Lucey¹, M.J. Hudson^{1,2*}, J. Steel¹

¹ *Department of Physics, University of Durham, Science Laboratories, South Road, Durham DH1 3LE, United Kingdom.*

² *Department of Physics & Astronomy, University of Victoria, P.O. Box 3055, Victoria BC V8W 3PN, Canada (Present address).*

15 July 2021

ABSTRACT

We present new spectroscopic and photometric data for 137 early-type galaxies in nine clusters, and for a set of nearby standard galaxies. The clusters studied are Perseus (A0426), Pisces, A0262, A0347, J8, HMS0122+3305, 7S21, A2199 and A2634.

Our spectroscopic data comprise radial velocities (cz), central velocity dispersions (σ) and magnesium line strength indices (Mg_2). Internal errors (derived from repeat observations) are 7.6 per cent on each measurement of velocity dispersion, and 0.010 mag. on each Mg_2 measurement.

Following Jørgensen et al., we correct our σ and Mg_2 results to a physical aperture size of $1.19h^{-1}\text{kpc}$. We correct the major published datasets to the same aperture size, and define a new ‘standard system’ by the aperture-corrected Lick data of Davies et al. Through extensive intercomparisons with data from the literature, we present the corrections required to bring the major published datasets onto the standard system. The uncertainty in these corrections is computed. We demonstrate that our new velocity dispersion data can be brought into consistency with the standard system, to an uncertainty of $\lesssim 0.01$ dex.

From R-band CCD photometry, we derive effective diameter (A_e), mean surface brightness within effective diameter ($\langle\mu\rangle_e$) and an R-band diameter equivalent to the D_n parameter of Dressler et al. Internal comparisons indicate an average error of 0.005 in each measurement of $\log D_n$. The combination $\log A_e - 0.3\langle\mu\rangle_e$, approximately the quantity used in the Fundamental Plane distance indicator, has an uncertainty of 0.006 per measurement. The photometric data can be brought onto a system consistent with external data at the level of 0.5 per cent in distance.

These data will be used in a companion paper, to derive distance and peculiar velocity estimates for the nine clusters studied.

Key words: galaxies: clusters: general — galaxies: elliptical and lenticular, cD — galaxies: distances and redshifts — galaxies: fundamental parameters

1 INTRODUCTION

Streaming motions of galaxies are the only probe of the large-scale distribution of mass in the nearby Universe. The dominant large-scale concentrations of galaxies within a distance of 8000 km s^{-1} are the Hydra–Centaurus/Great Attractor (hereafter GA) region and the Perseus–Pisces (hereafter PP) region (Saunders et al. 1991; Hudson 1993).

Strong infall into a massive concentration behind the Cen30 cluster was first claimed by Lynden-Bell et al. (1988). While there is clearly a coherent streaming motion of galax-

ies in the direction of Centaurus, it remains unclear whether this motion is generated locally by the GA, or whether more distant sources are responsible. The bulk streaming motion of the PP supercluster allows a test of these competing flow models. The GA infall model predicts the peculiar velocity of PP to be $\sim -100\text{ km s}^{-1}$. Alternatively, if more distant sources are responsible for the large peculiar motions in the Hydra–Centaurus direction, then PP might be expected to take part in a similarly large, but negative, bulk motion of $\sim 500\text{ km s}^{-1}$.

Previous work on motions in PP has been based mainly on application of the Tully & Fisher (1977) relation to samples of spiral galaxies. Using a field-spiral sample, Willick (1990, 1991) claimed that the PP supercluster was moving

* CITA National Fellow.

towards the local group (and therefore towards the GA) at 441 km s^{-1} . Willick quotes only a random error of 49 km s^{-1} but the study is also subject to a systematic calibration error of $\sim 100 \text{ km s}^{-1}$. Han & Mould (1992) analysed a sample of spirals in clusters, and reported an average peculiar motion of -400 km s^{-1} for PP, in close agreement with Willick.

As compared to the spiral data, the PP region was not well-sampled in the elliptical galaxy survey of Faber et al. (1989, 7S). To date, no extensive application of the $D_n - \sigma$ / Fundamental Plane (FP) method has been conducted in this region.

In this paper we present new spectroscopic and photometric parameters for a sample of early-type galaxies in 7 PP clusters. In a companion paper (Hudson et al. 1997; hereafter Paper II) we apply the $D_n - \sigma$ and FP relations to deduce distances and peculiar velocities of the clusters.

Our strategy of observing cluster galaxies is motivated by the recognition that a field sample suffers from severe homogeneous and inhomogeneous Malmquist bias, particularly in the vicinity of large structures such as PP (Hudson 1994). The magnitude of this bias can be reduced by grouping galaxies into clusters. The dominance of early-type galaxies in cluster cores ensures that samples are fairly robust against contamination from the field.

The acquisition of elliptical galaxy data in the PP region will also extend the volume over which one may assess the consistency of elliptical galaxy FP/ $D_n - \sigma$ distances, as compared to Tully-Fisher distances for spirals. This comparison may reveal that the distance indicator relations are affected by systematic variations associated with environmental effects or star-formation history (see, for example, Guzmán et al. 1992, Gregg 1995). Kolatt & Dekel (1994), using a preliminary version of the Mark III compilation of velocity data (Willick et al., 1997), have shown that the motions are consistent with the hypothesis that spirals and ellipticals trace the same velocity field. This compilation is limited, however, by the less extensive data available for ellipticals. The aim of the present work is to provide new, high-quality data for ellipticals in PP clusters, for use in mapping the velocity field with the FP method.

The present paper is organised as follows. Section 2 describes the sample selection. In Section 3, details are given of the spectroscopic observations and data reduction. Particular attention is paid to the construction of a ‘standard system’ of velocity dispersion measurements, and the estimation of systematic errors in the merged data. The photometric data and reduction are described in Section 4. Section 5 concludes the paper with a summary of the data quality in terms of random and systematic errors.

2 SAMPLE SELECTION

2.1 Selection of cluster sample

We define as PP the region of the sky bounded by the limits $0^{\text{h}} < \alpha < 4^{\text{h}}$ and $+20^\circ < \delta < +45^\circ$. It should be noted that this definition is not identical to that of Willick (1990, 1991), whose PP region extends from $22^{\text{h}} \lesssim \alpha \lesssim 3^{\text{h}}$. Within this region, the prominent clusters chosen for study were: Perseus (A0426), Pisces, A0262, A0347, J8, HMS0122+3305, 7S21. Of these, J8 (Jackson 1982) lies in the background of the PP

ridge, at $\sim 10000 \text{ km s}^{-1}$, while the remaining six form part of the main body of the supercluster, at $4000\text{--}6000 \text{ km s}^{-1}$. In addition, the clusters A2199 and A2634, which do not lie inside the PP region, were observed as part of an effort to resolve the conflict between estimates of their distances (Lucey et al. 1991a, 1993, 1997). Clusters A0262, A2199, A2634 and J8 have also been observed as part of the EFAR survey (Wegner et al. 1996).

Figure 1 shows the projected distribution of galaxies in the PP region, and slightly beyond in order to show also the position of A2634. Galaxy positions are from the CfA redshift survey (Huchra, 1993). Only those with radial velocities less than 12000 km s^{-1} are plotted. The positions of our target clusters are marked by open circles. The redshift-space distribution, for galaxies in $+20^\circ < \delta < +45^\circ$, is illustrated by Figure 2.

2.2 Selection criteria for cluster members

Galaxies were selected in a cone centred on each cluster position. The angular radius of each cone was chosen to give a physical radius of $1.0\text{--}2.5h^{-1} \text{ Mpc}$ at the cluster, using the distance suggested by the cluster redshift in the CMB frame. In Table 1 we summarise the selection criteria used in each cluster.

For Pisces, A0262, HMS0122+3305, and J8, objects were selected from APM scans (see Irwin & McMahon 1992). The images of all objects brighter than $B = 16$ ($B = 17$ for the more distant cluster J8) were inspected, using Palomar Sky Survey material. An initial inspection served to discriminate galaxies from close pairs of stars, merged galaxies and plate defects. In merged objects containing one or more galaxy, the magnitude of each galaxy was estimated by eye, given the total magnitude of the system. All galaxies were examined and morphological types were assigned. Only E and S0 galaxies without prominent disks were retained in the final sample. The remaining galaxies were cross-referenced with known objects at similar positions, using NED[†]. Those with literature redshifts different by more than 2000 km s^{-1} from the nominal cluster redshift were deleted from the sample.

For 7S21 and A0347, APM scans were not available at the time of selection. The HST Guide Star Catalogue was used to select non-stellar objects in these clusters. Suitable candidates were then selected and typed by inspection of sky survey plates, and cross referenced with NED.

For galaxies in the Perseus cluster, which lies at low galactic latitude, reliable E and S0 galaxies were selected from the work of Poulain, Nieto & Davoust (1992). A few extra ellipticals were added from the 7S sample.

For A2199 and A2634, galaxies were selected from Lucey et al. (1991a).

For most of the galaxies for which data is presented here, reliable positions are available through NED. Cross references are provided, with our data, to a reference number from well known catalogues (NGC, IC, UGC, CGCG) or from more specialist papers: Chincarini & Rood (1971, CR); Bucknell, Godwin & Peach (1979, BGP); Dressler (1980);

[†] NED, the NASA/IPAC extragalactic database, is operated for NASA by the Jet Propulsion Laboratory at Caltech.

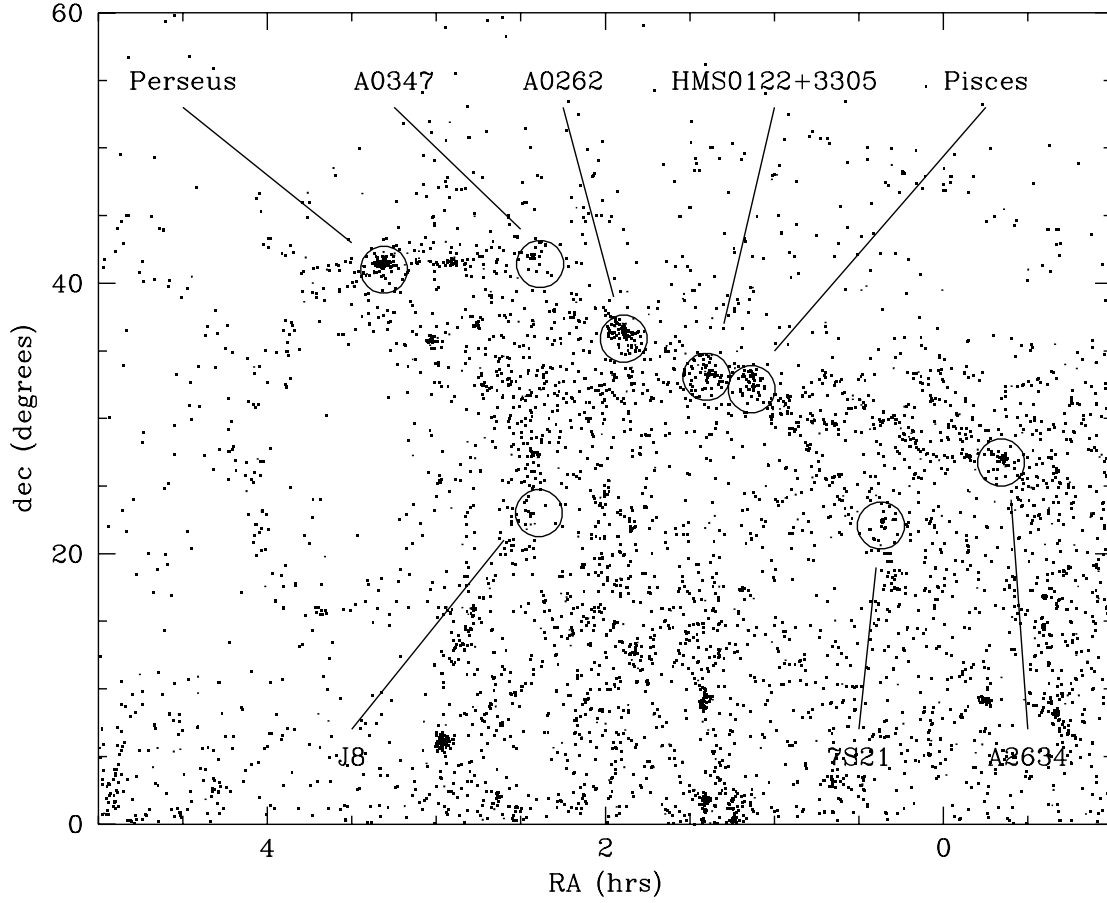


Figure 1. Projected distribution of CfA survey galaxies (with $cz < 12000 \text{ km s}^{-1}$, in the direction of PP. Clusters studied in this work are identified by open circles. The circle size is not significant. A2199 lies at $\alpha = 16^{\text{h}}27^{\text{m}}$; $\delta = +40^\circ$, and is not shown. The low density of galaxies north of $+40^\circ$ is a result of the limited range of the Arecibo radio telescope. East of Perseus, obscuration by the galactic plane is apparent.

Table 1. Selection criteria for galaxies in each of the PP region clusters. cz_{nom} is the CMB-frame redshift used in calculating the projected physical radius, R_{proj} at the distance of each cluster. Under ‘source’, we refer to the catalogue and plate material used for visual inspection of candidates.

Cluster	RA (B1950)		Dec (B1950)		cz_{nom} km s^{-1}	Search radius	R_{proj} $h^{-1}\text{Mpc}$	magnitude	Source
7S21	00	18.6	+22	05	5500	1°	1.0	$B \sim 16$	GSC + POSS II
Pisces	01	04.5	+32	10	4700	2°	1.6	$B = 16$	APM + POSS I
HMS0122+3305	01	20.5	+35	10	4600	2°	1.6	$B = 16$	APM + POSS I
A0262	01	49.9	+35	54	4500	2°	1.6	$B = 16$	APM + POSS I
A0347	02	19.6	+41	25	5300	1.5°	1.4	$B \sim 16$	GSC + POSS II
J8	02	26.0	+23	00	9800	1.5°	2.5	$B = 17$	APM + POSS I
Perseus	03	15.0	+41	00	4800	1°	0.8	$B = 17$	Poulain + 7S

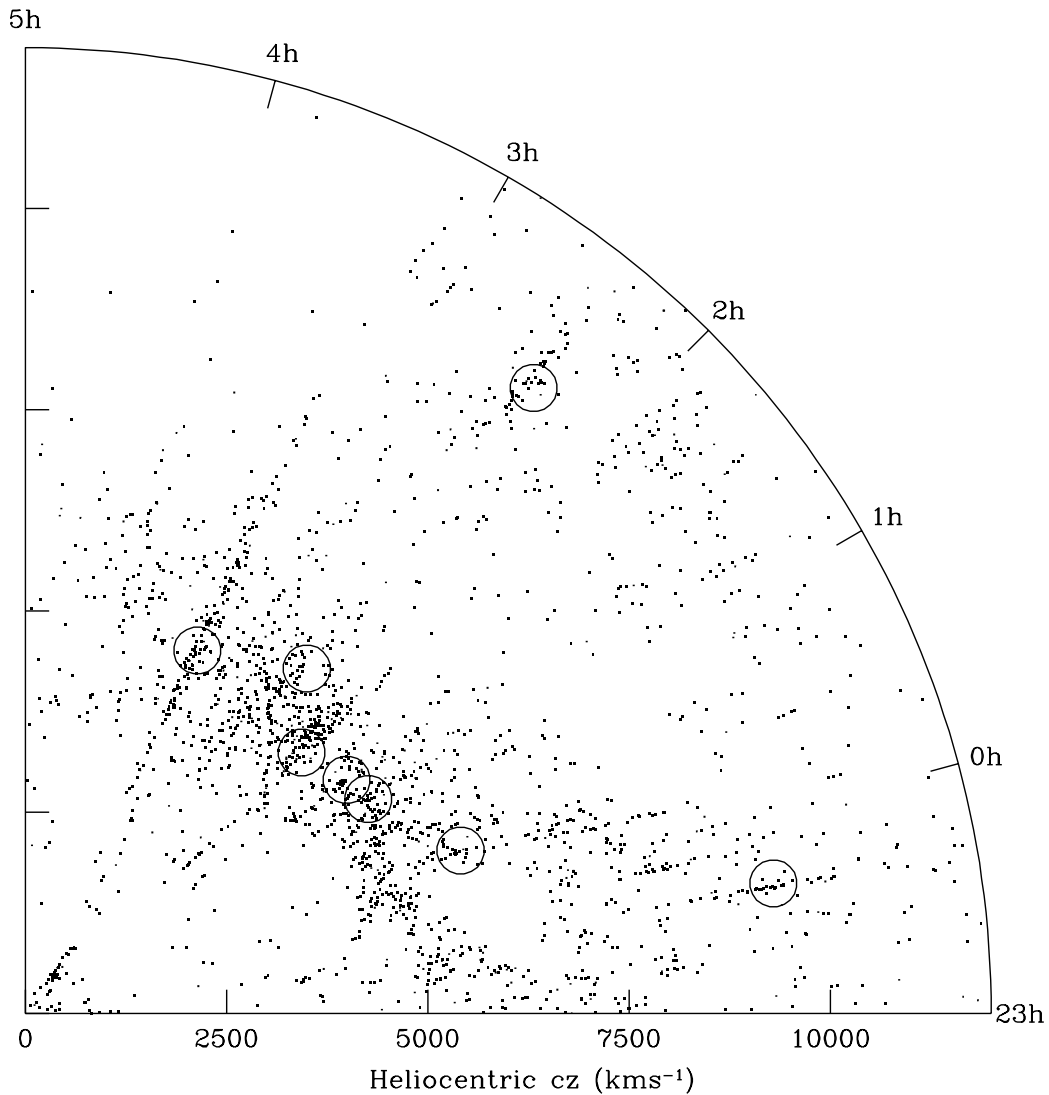


Figure 2. Redshift space distribution of CfA survey galaxies in declination range $20^\circ < \delta < +45^\circ$. Clusters to be studied here are marked by open circles. A2199 lies well beyond the limits of this plot, at 16.5^{h} RA.

Faber et al. (1989); Lucey et al. (1991a); Wegner et al. (1996). In Table 2, we list positions for the galaxies not included in the above lists.

As in most programmes of peculiar velocity measurement, the selection criteria described here are somewhat inhomogeneous in terms of limiting magnitudes. This non-uniformity would result in biases in the cluster distances if not handled correctly. Methods for deriving unbiased $FP/D_n - \sigma$ relations and distances will be discussed and applied in Paper II.

Note also that morphological selection from sky survey plates is necessarily subjective. Andreon (1994) has reported that, for galaxies in the Poulain et al. sample, around a half of those classified as E by visual inspection of survey plates have Poulain et al. types S0 or later.

3 SPECTROSCOPY

3.1 Observations

Spectroscopic observations were made using the 2.5m Isaac Newton Telescope (INT) on La Palma, in 1993 and 1994. Different detectors were used in each run : an EEV CCD in 1993, and the faster TEK CCD in 1994. An EEV chip was used for one night of the 1994 run, due to technical problems. This resulted in three spectroscopic datasets (hereafter denoted EEV93, EEV94, TEK94), which were each treated separately during the course of the data reduction. Instrumental details for the three datasets are summarised in Table 3.

Table 3. Spectroscopic instrumentation.

Dataset	EEV93	EEV94	TEK94
Dates	Nov. 15–22, 1993	Sep. 6, 1994	Sep. 3–5 & 7–9, 1994
Observers	JRL, MJH, JS	JRL, JS	JRL, JS
Telescope	2.5m INT	2.5m INT	2.5m INT
Spectrograph	IDS	IDS	IDS
Wavelength Range	4760–5784Å	4760–5784Å	4760–5784Å
Slit size	3 arcsec	3 arcsec	3 arcsec
CCD	EEV	EEV	TEK
CCD Dimensions	1242×1152	1242×1152	1024×1024
Effective aperture	3.0×3.3 arcsec	3.0×3.3 arcsec	3.0×3.5 arcsec
Number of Galaxy Spectra	105	16	211
Mean seeing	1.5 arcsec	1.5 arcsec	1.2 arcsec

Table 2. Positions for uncatalogued galaxies in the PP sample. For all other galaxies studied here, positions are available through NED.

Cluster	Our name	RA (B1950)	Dec (B1950)
7S21	S06	00 18 44.8	+21 42 22
Pisces	Z17005	00 56 43.0	+32 52 04
	Z16012	00 59 04.2	+33 20 51
	Z01047	01 04 12.4	+32 02 30
	Z01032	01 05 27.0	+32 11 13
	Z04035	01 05 43.7	+33 06 58
	Z10020	01 09 05.1	+31 17 37
HMS0122+3305	H01027	01 21 00.9	+33 19 29
A0262	A14050	01 47 18.8	+35 58 52
	A01094	01 47 26.5	+35 44 09
	A01076	01 49 36.2	+35 52 08
A0347	B03C	02 20 01.9	+42 45 54
J8	J07038	02 24 03.4	+23 24 06
	J09035	02 24 41.2	+21 45 40
	J08035	02 24 41.4	+22 51 39
	J01065	02 25 49.1	+22 47 23
	J03049	02 26 52.2	+23 44 03
	J01055	02 26 59.2	+22 53 12
	J01080	02 27 46.0	+22 29 54

3.2 Derivation of spectroscopic parameters

Initial reduction of the CCD frames involved bias and dark current subtraction, the removal of pixel-to-pixel sensitivity variations (using flat field exposures provided by a tungsten calibration lamp) and correction for vignetting along the slit (using twilight sky-line exposures).

The spectra obtained covered $\sim 1000\text{\AA}$ centred on the Mg b triplet, and were sampled with a resolution of $\sim 4\text{\AA}$ FWHM.

Wavelength calibration was performed using arc-lamp exposures, taken regularly in the course of the observations, and always after movement from one cluster or region to another. A cubic fit between pixel number and wavelength for ~ 18 arc lines gave a maximum rms calibration error of $\sim 0.1\text{\AA}$.

Spectra were extracted from the frames by simple co-addition of the central 5 rows of the galaxy. The resulting effective aperture size is tabulated for each dataset in Ta-

ble 3. After application of a median-filter to remove cosmic ray events, the darkest rows on the frame were used to produce a sky spectrum.

For some galaxies in the EEV93 dataset, sufficient signal-to-noise could be obtained only by co-adding spectra resulting from two separate exposures. In almost all of these cases, the two exposures were taken in immediate succession, ensuring the validity of the co-addition.

Cosmic ray events in the galaxy spectra were removed by a combination of automatic procedures before extraction, and interactive methods applied at the one-dimensional spectrum stage. Features in the spectrum resulting from noise in the subtraction of sky-line features (especially at 5577\AA) were similarly removed after extraction.

On each run, spectra were obtained for several G8 to K3 giant stars, for use as template spectra. These stars were trailed across the slit at a shallow angle during the exposure, to produce an extended illumination. Subsequent weighting of these frames, by a typical galaxy profile, effects a simulated observation of a galaxy with zero velocity dispersion. The extension of illumination has the effect of broadening the stellar spectra by $\sim 30\text{ km s}^{-1}$.

The method used for measurement of the velocity dispersion, σ , for each galaxy, is based upon the well-known Fourier Quotient method of Sargent et al. (1977). In preparation for the application of this procedure, continuum levels were subtracted from both the template spectrum and the galaxy spectrum, and both were submitted to a cosine bell modulation to fix the spectrum ends to zero. The latter step is necessary to avoid unphysical signals appearing at all frequencies in the Fourier Transforms.

The method requires also the removal from the spectra of signals resulting from noise, inadequate continuum removal and the application of the cosine bell. Firstly, a cut is made at high frequencies, to remove noise. The results of this method seem to be fairly insensitive to the exact value, k_{high} , chosen for the high frequency cut. $k_{\text{high}} = 200 \approx (5\text{\AA})^{-1}$ has been used throughout. Furthermore, a low frequency filter must be applied to remove residual continuum features, and the effects of the cosine-bell modulation function described above. With the low-frequency cut, however, results are found to exhibit a clear trend: velocity dispersions are measured to be smaller when k_{low} is higher. One must choose the cutoff frequency with care. The highest sensible k_{low} is that which would preserve spectral features in spectra of velocity dispersion $\leq 500\text{ km s}^{-1}$. This is $k_{\text{low}} = 9 \approx (110\text{\AA})^{-1}$ for our spectra. The lowest sensible k_{low} is that

which is necessary to remove the signal of the cosine-bell modulation. This is $k_{\text{low}} = 6 \approx (170\text{\AA})^{-1}$ for our spectra. The portion of the $\sigma - k_{\text{low}}$ plot between these sensible limits is flat to ~ 5 per cent for most galaxies.

After discarding a few template spectra which gave consistently discrepant results, the velocity dispersions were averaged over 13 template spectra of 6 different stars, and over values $k_{\text{low}} = 6, 7, 8, 9$ adopted for the low frequency filter.

The uncertainty on each velocity dispersion was quantified by repeatedly conducting the measurement after bootstrap resampling of the spectrum. This provides an estimate of the random, Poisson-noise error on σ .

Recession velocities (cz) were obtained simultaneously with velocity dispersions, as a result of the Fourier Quotient fit.

The Mg_2 line strength index for the magnesium feature was also derived for each spectrum. In order to calculate this index, independent of the shape of the instrumental response curve, the spectra were first flux-calibrated by reference to spectrophotometric standard stars observed during the runs. For certain observations, no appropriate flux-standard was obtained, so a few galaxies have no Mg_2 measurement. Initial flux calibration of the EEV93 data was found to be unsatisfactory, due to a strong gradient in chip response across the spectral region being used. The calibration was improved by an extra step in which we derived the response curve of the EEV relative to the TEK, using a star common to both datasets, before calibrating to the absolute standard of flux. A similar problem for the EEV94 data could not be resolved in this manner, since there are no stars in common between that dataset and the TEK94 data. As a result there are no Mg_2 measurements from the EEV94 observations. Uncertainties in the Mg_2 indices were calculated simply from the noise characteristics of the chip employed.

3.3 Raw spectroscopic data and internal comparisons

Table 11 presents the raw spectroscopic data obtained, including formal errors. Over half of the galaxies were observed more than once. Comparisons between repeat measurements in the two large datasets (EEV93 and TEK94) are illustrated in Figures 3 and 4 for velocity dispersion and Mg_2 index, respectively. Note that there are no repeat observations within the small EEV94 dataset. The implied observational errors in each dataset are summarised in Table 4. Weighting the σ uncertainties in TEK94 and EEV93 by the number of observations in each dataset, we obtain a typical measurement error of 0.032 dex per measurement.

For comparison, the 7S Lick data exhibit an internal uncertainty of 0.057 dex in σ . The higher quality 7S velocity dispersions are accurate to 0.036 dex (Davies et al.). The mean Poisson error on σ is 0.023 dex (TEK94) and 0.029 dex (EEV93). Non-Poissonian effects therefore account for an appreciable portion of the observed scatter, especially for the earlier dataset.

Uncertainties on the Mg_2 measurements are typically 0.010 mag., and are fully accounted for by the mean photon-noise error.

Table 4. Uncertainties in the EEV93 and TEK94 datasets, as judged from the scatter of repeat measurements. For each parameter, N indicates the number of galaxies for which comparisons could be made.

Dataset	N	rms $\Delta(\log \sigma)$	N	rms $\Delta(\text{Mg}_2)$	N	rms $\Delta(cz)$
TEK94	48	0.027	44	0.010	48	31.2
EEV93	20	0.041	20	0.011	20	23.1

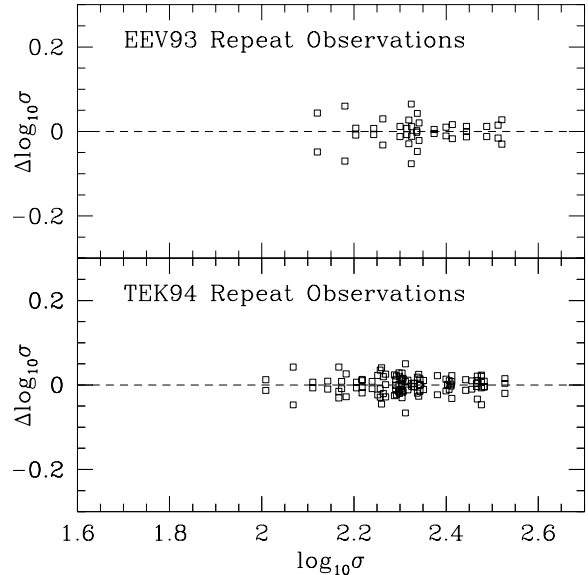


Figure 3. Scatter of repeat velocity dispersion measurements within the datasets presented here. In each panel, the horizontal axis is the mean quantity derived from the dataset; the vertical axis is the deviation of each individual measurement from that mean. Note that there are no internal repeats within the EEV94 dataset. For ease of comparison, the axis limits for this plot are the same as for the equivalent plot in Davies et al. (1987)

3.4 The aperture correction

The physical size of that central part of a galaxy, observed through a fixed aperture, is larger for a more distant galaxy than for one nearby. Since galaxies, in the mean, exhibit a negative radial gradient in both $\log \sigma$ and Mg_2 , a correction must be applied to the raw data before use. Furthermore, to compare measurements made using different aperture sizes, a similar correction is clearly necessary. Jørgensen, Franx & Kjaergaard (1995b) present an analysis based on the observed radial gradients in $\log \sigma$ and Mg_2 for nearby galaxies. They find that a power law provides an adequate description of the required correction:

$$\log \frac{\sigma_{\text{corr}}}{\sigma_{\text{obs}}} = 0.04 \log \frac{r_{\text{ap}}}{r_{\text{norm}}} \quad (1)$$

where r_{ap} is the physical radius sampled by that circular aperture from which one obtains the same σ_{obs} as through the actual aperture used. For a rectangular aperture of angular dimensions x and y (in radians), and a galaxy at distance d , the equivalent aperture is

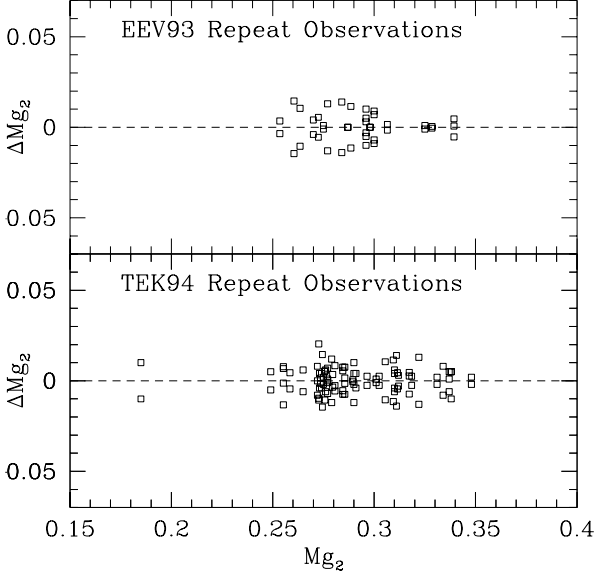


Figure 4. As for Figure 3, but for Mg_2 index measurements.

Table 5. Run-to-run comparisons of spectroscopic data. N indicates the number of galaxies involved in each comparison.

Comparison	N	Mean $\Delta(\log \sigma)$	Dispersion
EEV93 – TEK94	46	-0.009 ± 0.006	0.042
EEV94 – TEK94	10	0.014 ± 0.012	0.039

Comparison	N	Mean $\Delta(Mg_2)$	Dispersion
EEV93 – TEK94	46	-0.010 ± 0.002	0.013

$$r_{\text{ap}} \approx 1.025 \left(\frac{xy}{\pi} \right)^{1/2} d \quad (2)$$

where the correction factor 1.025 is included to provide an improved match to more detailed models. An independent analysis, based on measured velocity dispersion profiles, supports the size of this correction.

For the normalisation, we follow Jørgensen et al. in adopting a physical diameter $2r_{\text{norm}}$ of $1.19 h^{-1} \text{kpc}$. This is equivalent to an angular diameter of 3.4 arcsec for Coma cluster galaxies.

Jørgensen et al. find the average radial gradient of the Mg_2 index to be so similar to that of the velocity dispersion, that equation 1 may be used for the Mg_2 aperture correction, with a simple substitution of Mg_2 for $\log \sigma$.

3.5 Matching of spectroscopic datasets onto a new ‘standard system’

In order to construct large samples of peculiar velocity data, we require that velocity dispersions measured at different telescopes match as accurately as possible. At the PP distance, a one per cent systematic error in σ corresponds to 50 km s^{-1} in peculiar velocity. A systematic difference between the velocity dispersions measured on telescopes in opposite hemispheres would thus generate a spurious bulk flow. Despite careful attempts to correct the velocity dispersions for aperture effects, systematic differences between velocity dis-

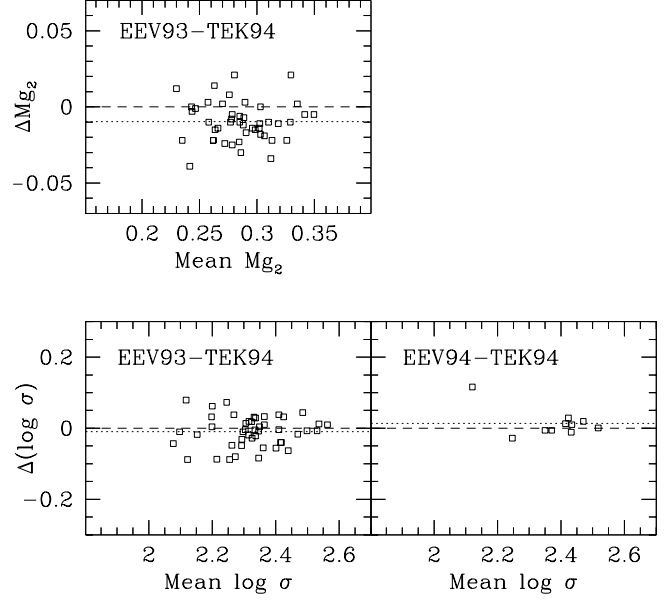


Figure 5. Comparison between spectroscopic parameters derived from the three datasets presented in this paper. The data are aperture corrected, but nevertheless exhibit systematic offsets from run to run, as shown by the dotted lines. The offsets are quantified in Table 5.

persions measured from different datasets persist at the ~ 3 per cent level. Such offsets are present even between the three datasets presented here (as illustrated in Figure 5 and Table 5), despite the use of very similar observational methods and data reduction techniques.

The removal of systematic offsets can be achieved by intercomparison of results for galaxies common to two or more systems. To this end, our data include many galaxies observed to improve overlap with existing systems. In this section, we consider velocity dispersion and Mg_2 data on 19 and 16 different systems, respectively. In order to take account of zero-point differences reported by Dressler (1984), the 7S LCOHI data have been subdivided into the three constituent runs from which they derive.

Many galaxies have measurements on more than two systems. Therefore in order to determine self-consistent corrections between different systems, a simultaneous fit for all of the offsets is necessary. The fit is performed using velocity dispersion and Mg_2 data corrected to the Jørgensen et al. (1995b) standard physical aperture size of $1.19 h^{-1} \text{kpc}$. We determine the corrections necessary to bring all systems into the best possible agreement with each other. We adopt the fully-corrected Lick system (Davies et al. 1987) as the standard and determine the remaining corrections as follows. Let $s = \log_{10}(\sigma)$ and let i, j and k index the measurement, galaxy and system respectively. We obtain the corrections Δ_k , needed to bring each system into agreement with Lick, by minimising a χ^2 statistic

$$\chi^2 = \sum_i \frac{(s_i + \Delta_k - \bar{s}_j)^2}{e_k^2} \quad (3)$$

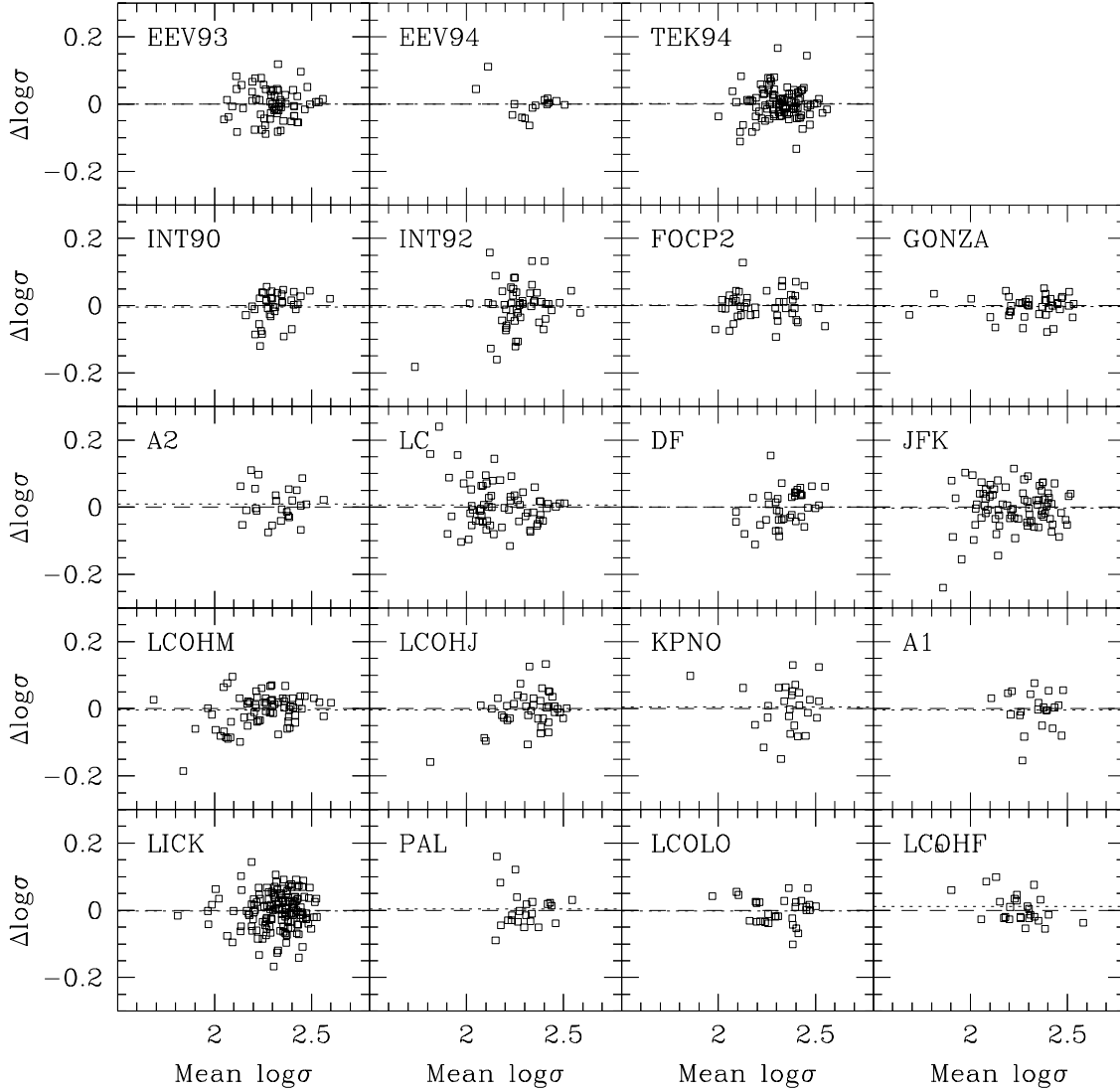


Figure 6. Consistency of the merged system of velocity dispersion measurements. For the each galaxy in the TEK94 panel, we compute the mean (fully corrected) TEK94 measurement, and the mean (fully corrected) value using all the other data – excluding TEK94. We plot as $\Delta \log \sigma$ the difference between the ‘TEK94-only’ and the ‘all-but-TEK94’ values. All 19 velocity dispersion systems are treated in this way. Note that we include in these plots all measurements, including those which were not used in the derivation of the corrections. The small offsets still present in some plots (indicated by dotted lines) are a result of these outlying points and low σ galaxies.

where e_k is the error in s_i (assumed to be the same for all galaxies in a given system) and \bar{s}_j is the error-weighted mean of all corrected measurements of the same galaxy.

We determine the errors e_k for each system by adjusting these so that the reduced χ^2 is unity, both when the system is included and when it is excluded from the comparisons. This external error (e_{ext}) is typically 10 – 25 per cent larger than the internal error (e_{int}) estimated from repeat measurements on the same system.

The overlap data set of velocity dispersion measurements (galaxies with velocity dispersions on more than one system) consists of 1281 measurements for 350 different galaxies. We exclude galaxies with $\bar{s} < 2$ as these may be

subject to large random and systematic errors (Jørgensen et al. 1995b). We also exclude individual velocity dispersion measurements which are inconsistent at the 3.5σ level with the other measured velocity dispersions of the same galaxy. The velocity dispersions so excluded are A2634-F1201 (EEV93 $s = 2.0784$), A1656D-136 (INT90 $s = 2.0888$), N386 (KPNO $s = 1.7923$), N548 (LICK $s = 1.8856$) and VELA-G22 (FOCP2 $s = 1.9237$).

The overlap data set of Mg_2 measurements (galaxies with measurements on more than one system) consists of 1013 measurements of 270 different galaxies on 16 systems (the LC, FOCP2 and EEV94 systems have no Mg_2 data). In addition to the galaxies excluded in the velocity dispersion

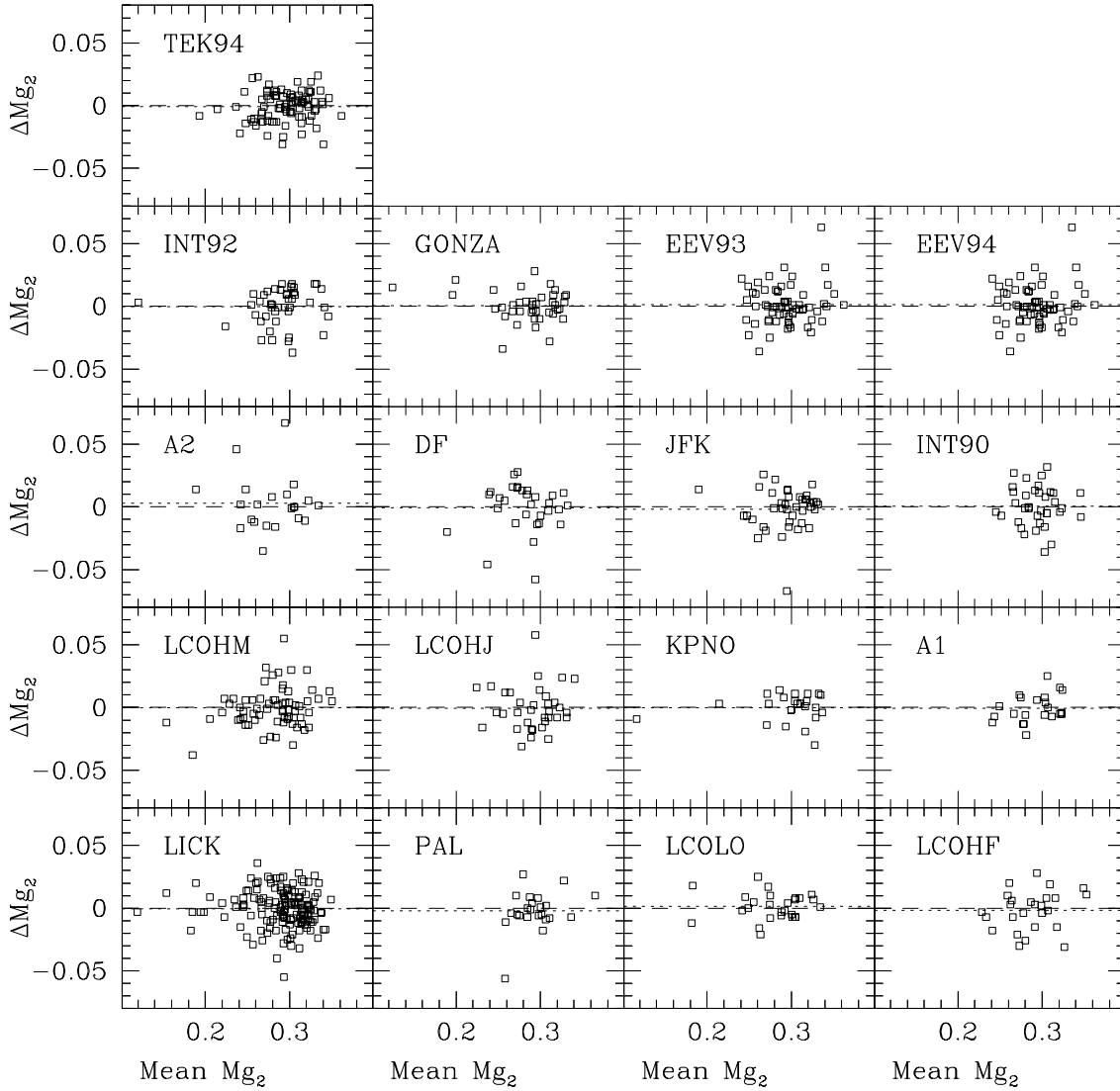


Figure 7. As for figure 6, but for the 17 systems of Mg_2 measurements.

comparison, we also exclude the following data which are inconsistent with other measurements of the same galaxy at the 3.5σ level: N1282 (PAL $Mg_2 = 0.0245$), N1549 (A2 $Mg_2 = 0.342$ and JFK $Mg_2 = 0.264$) N4564 (EEV93 $Mg_2 = 0.350$) and N6702 (GONZA $Mg_2 = 0.243$ and TEK94 $Mg_2 = 0.288$).

Tables 6 and 7 summarise the required corrections to velocity dispersion and Mg_2 , respectively. Note that, because of the interdependencies between the different corrections, the simple pair offsets of Table 5 are not trivially related to those derived here by simultaneous fits. In Figures 6 and 7 we illustrate the level to which systematic offsets are removed by the application of the derived corrections.

The errors are determined by bootstrap resampling the master data file and computing the corrections from the re-sampled file. This procedure allow us to determine not only the error on the correction to each system but also the cor-

relation between the corrections for different systems. Using the bootstrap values of these corrections, we can generate mock merged data sets and so determine for a given cluster the error in the mean correction. This is an estimate of the mean systematic error in s , which will generally depend on the systems merged for the cluster, their relative proportions and their covariance. For the PP sample, we find that for all clusters this error is ~ 1.5 per cent in σ . This translates to a systematic error of ~ 2 per cent in distance, or $\sim 100 \text{ km s}^{-1}$ at PP.

3.6 Correction and combination of spectroscopic data

In this section, we briefly summarise the recipe for converting the raw spectroscopic data tables into the corrected and

Table 6. Corrections required to bring each system of (aperture-corrected) velocity dispersion measurements into agreement with the standard system. e_{Δ} are the errors on each correction. N_{ov} represents, for each system, the number of galaxies in the overlap dataset, ie having measurements on other systems.

Name	Source	N	e_{int}	e_{ext}	Δ	e_{Δ}
LICK	1	276	0.052	0.055	$\equiv 0$	$\equiv 0$
PAL	2	23	–	0.045	–0.0241	0.0116
LCOLO	1	61	0.039	0.040	0.0115	0.0098
LCOHF	3	25	–	0.035	–0.0067	0.0105
LCOHM	3	73	0.023	0.035	0.0106	0.0072
LCOHJ	3	61	0.021	0.035	0.0021	0.0086
KPNO	1	27	–	0.065	0.0142	0.0139
A1	1	27	0.024	0.040	–0.0057	0.0113
A2	1	42	0.036	0.045	0.0176	0.0102
LC	4	72	0.033	0.035	–0.0127	0.0096
DF	5	41	–	0.044	–0.0038	0.0112
JFK	6	76	–	0.040	0.0011	0.0089
INT90	7	59	0.038	0.040	–0.0177	0.0094
INT92	8	60	0.040	0.055	0.0080	0.0096
FOCP2	9	67	0.034	0.035	–0.0063	0.0094
GONZA	10	38	–	0.014	0.0222	0.0054
EEV93	11	86	0.040	0.040	–0.0014	0.0082
EEV94	11	15	–	0.040	–0.0115	0.0111
TEK94	11	152	0.027	0.030	–0.0063	0.0059

Sources:

- 1 – Davies et al. (1987)
- 2 – Davies et al. (1987) – Palomar observations wrongly attributed to LCOHI dataset (see Dressler et al. 1987)
- 3 – Davies et al. (1987) LCOHI data subdivided according to run: Feb. 82 (LCOHF); Mar. 83 (LCOHM) and Jan. 84 (LCOHJ)
- 4 – Lucey & Carter (1988)
- 5 – Dressler, Faber & Burstein (1991)
- 6 – Jørgensen, Franx & Kjærgaard (1995b)
- 7 – Lucey, Guzman, Carter & Terlevich (1991)
- 8 – Lucey, Guzman, Steel & Carter (1997)
- 9 – Lucey et al. (1998)
- 10 – Gonzales (1993)
- 11 – This paper

Table 7. As for Table 6, but for Mg₂ measurements.

Name	Source	N	e_{int}	e_{ext}	Δ	e_{Δ}
LICK	1	274	0.008	0.011	$\equiv 0$	$\equiv 0$
PAL	2	22	–	0.014	–0.0143	0.0026
LCOLO	1	53	0.011	0.010	–0.0032	0.0024
LCOHF	3	24	–	0.013	–0.0139	0.0046
LCOHM	3	68	0.004	0.013	–0.0086	0.0023
LCOHJ	3	53	0.007	0.013	–0.0185	0.0029
KPNO	1	24	–	0.011	–0.0034	0.0028
A1	1	27	0.012	0.009	0.0074	0.0029
A2	1	33	0.005	0.010	–0.0132	0.0034
DF	5	31	–	0.017	–0.0035	0.0040
JFK	6	40	–	0.011	–0.0017	0.0024
INT90	7	54	0.012	0.015	0.0061	0.0030
INT92	8	51	0.013	0.012	0.0168	0.0027
GONZA	10	37	–	0.007	–0.0048	0.0017
EEV93	11	83	0.010	0.012	0.0172	0.0021
TEK94	11	139	0.009	0.009	0.0071	0.0016

Sources as in Table 6.

combined measurements to be used in the peculiar velocity analyses.

In order to combine multiple σ and Mg₂ observations for a galaxy, it is first necessary to ensure that all the sources of data are on a consistent system. To this end we correct the EEV93, EEV94 and TEK94 systems for aperture effects, and scale them onto our new ‘standard system’ using the offsets listed in Tables 6 and 7. The distance used in calculating the aperture correction is the median redshift of the relevant cluster, or (if not part of the cluster sample) the individual galaxy redshift.

The data for multiply-observed galaxies are then combined to give a weighted mean $\log \sigma$, and weighted mean Mg₂. The weight of each measurement is assigned according to the external error on the dataset from which it derives. In constructing the means, we exclude the ($> 3.5\sigma$) deviant measurements as flagged above.

It should be stressed that the external datasets (LICK, FOCP2, etc.) are used only to derive the necessary corrections, and to identify outlying measurements. The mean parameters are calculated using data drawn only from EEV93, EEV94 and TEK94.

Recession velocities are combined by correcting the EEV93 and EEV94 systems according to their offsets from TEK94, before computing a simple mean cz . The relative offsets are EEV93 – TEK94 = $-10 \pm 5 \text{ km s}^{-1}$ and EEV94 – TEK94 = $-4 \pm 10 \text{ km s}^{-1}$, derived from 45 and 10 galaxies respectively.

We have compared the resulting mean recession velocity measurements with those adopted by 7S (Faber et al. 1989, Davies et al. 1987). The median offset is $22 \pm 13 \text{ km s}^{-1}$, with our velocities being the larger. The comparison is displayed in Figure 8. The most discrepant point is galaxy N1272 (P17). For this galaxy, we have seven concordant measurements of cz .

Table 13 presents the fully corrected and combined spectroscopic data, scaled to the ‘standard’ system, for galaxies in the cluster sample. This table includes only those galaxies for which complementary photometric data has been obtained.

4 PHOTOMETRY

4.1 Introduction

The photometric observations were made in the Kron–Cousins R bandpass. For the $D_n - \sigma$ relation, we have defined the R-band D_n parameter to be that diameter which encloses a mean surface brightness $\langle \mu \rangle_R = 19.23 \text{ mag. arcsec}^{-2}$. If the typical (extinction- and k -corrected) $V - R$ colour for early-type galaxies is 0.57, as indicated by the BVR photometry of Colless et al. (1993), then our R-band D_n diameters will be well matched to the V-band system of Lucey et al. (1991b), and to the B-band work of Burstein et al. (1987). At the distance of the clusters studied here, the typical D_n diameter, so defined, is comfortably large compared to the seeing disk, yet not so large that sky subtraction errors become significant. The quantities measured for use in the FP distance indicator are the effective diameter A_e , and the mean surface brightness within effective diameter, denoted $\langle \mu \rangle_e$.

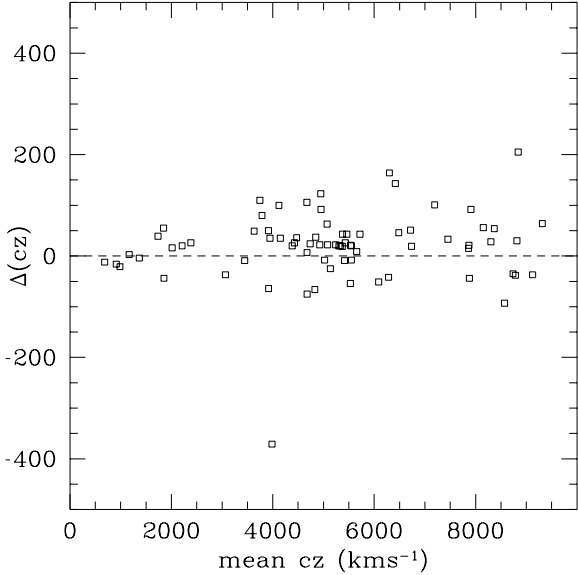


Figure 8. Comparison of our recession velocity measurements with the recession velocities adopted by 7S. We plot the difference in cz in the sense (‘This Study’ – 7S), against the mean of the two measurements. External data for 75 galaxies are drawn from Faber et al. (1989) and Davies et al. (1987). The discrepant point is for N1272.

4.2 Observations and initial data reduction

CCD photometry was obtained on the 1-m Jacobus Kapteyn Telescope (JKT) on La Palma in 1993 November and 1994 September. Table 8 summarises the instrumental configuration used. The observations were made with the RGO ‘Harris’ R filter which, in combination with a typical CCD response, provides a close match to the standard Kron–Cousins R bandpass. The images covered an area of 6.6×6.1 arcmin², at a scale of 0.31 arcsec pixel⁻¹. The initial reduction of the CCD images followed standard procedures of bias-subtraction and flat-fielding, using Starlink software. The photometric calibration was achieved by observations of Landolt (1983, 1992) standard stars and fields. At least 12 Landolt stars/fields were observed each night and an on-line assessment of photometric conditions was employed to track the stability of the atmospheric extinction. For the calibration mapping we used the equation,

$$R = r_{\text{inst}} + ZP - k_R X + C(B - V) \quad (4)$$

where R is Landolt’s listed R-band magnitude, $B - V$ is the listed colour, r_{inst} is the instrumental magnitude, X is the airmass, ZP is the photometric zero-point, k_R the R-band extinction per airmass and C is the colour term. We solved for the ZP , k_R and C terms by minimising the residuals. Five nights (out of a total 14 allocated) were photometric. The residual scatter of the standard stars on these nights was less than 0.015 mag. The k_R term was typically 0.10. The colour term, C , was only -0.011, confirming the excellent match of the RGO ‘Harris’ R filter to the standard Kron–Cousins R system. For the limited $B - V$ colour range of early-type galaxies in our study this colour term can be safely included in the zero-point term, and observations in R-band alone can be used. In order to assess the reliability

Table 8. Photometric Instrumentation

Dates	Nov. 15–22, 1993	Sep. 1–7, 1994
Observers	JRL, MJH, JS	JRL, JS
Telescope	1.0m JKT	1.0m JKT
CCD	EEV	EEV
CCD Dimensions	1280×1180	1280×1180
Pixel Scale	0.31 arcsec	0.31 arcsec
Filter	Harris R	Harris R

of our photometric measurements and run-to-run variations, a large number of our target galaxies were observed more than once (see below). FWHM seeing (measured from stellar profiles on the target galaxy images) ranged from 0.7 to 3.0 arcsec, with a typical value of 1.3 arcsec.

4.3 Derivation of photometric parameters

For each galaxy, circular aperture magnitudes were determined in diameter steps of approximately 0.1 dex from 4 arcsec out to ~ 60 arcsec. Contaminating stars and galaxies were removed interactively from each target galaxy. Aperture magnitudes were corrected for galactic extinction and for cosmological k -dimming. For the R-band extinction, we adopt $A_R = 2.35E(B - V)$ where $E(B - V)$ are the reddening values of Burstein & Heiles (1984). For the k -correction, we use $-1.0z$ (Oke & Sandage 1968, Frei & Gunn 1994). A correction for the $(1+z)^4$ surface brightness dimming is also applied.

To derive the parameters D_n , A_e and $\langle\mu\rangle_e$, we fit a de Vaucouleurs $R^{1/4}$ profile to the aperture photometry. Seeing effects in the aperture magnitudes cannot be ignored in this procedure, and are here corrected for by an improved version of the method first reported by Bower, Lucey and Ellis (1992). Whereas Bower et al. calculate the seeing corrections appropriate for a galaxy of true effective radius 5 arcsec, and apply these to all galaxies, we have compiled correction tables for a range of true radii, and use an iterative technique to select the table required for a given galaxy. Convergence to a corrected A_e value is very rapid. In practice this improved correction scheme leads to measurements which are in good agreement with those made using the original Bower et al. method. For only five images, out of a total 245, do we find D_n or FP parameters which change by more than 1 per cent (distance equivalent) in adopting the new corrections.

The typical rms residual from the $R^{1/4}$ law fit is 0.02 mag. The four worst-fit galaxies have residuals of 0.05–0.09 mag. rms. Saglia et al. (1997) have recently investigated the effect of fitting a pure $R^{1/4}$ law to galaxies with substantial disk components. They show that such a fit to a galaxy with disk-to-bulge ratio 0.2 can result in A_e measurements which are wrong by as much as 30%. Whilst this severely affects the determination of effective radius and of surface brightness, the combination $\log A_e - 0.3\langle\mu\rangle_e$ (which enters into the Fundamental Plane) is robust against the presence of a disk, since the errors on A_e and $\langle\mu\rangle_e$ are correlated. The D_n parameter, defined by interpolation of the data, rather than from a global profile fit, is also insensitive to this effect. We note also, that a bias in cluster distances will only result from this effect if, from cluster to cluster, substantially different morphological proportions are sampled.

The final fully-corrected photometric parameters are

Table 9. External comparison of aperture photometry with R-band work from other sources. Offsets are given in the sense ‘this work’ – ‘literature’.

Source	N_{gal}	Mean offset	Dispersion
Steel (1997)	22	-0.002 ± 0.010	0.047
Postman & Lauer (1995)	5	-0.025 ± 0.011	0.026
Colless et al. (1993)	17	-0.037 ± 0.007	0.032

presented in Table 12. For comparison with future work, we tabulate also the uncorrected R-band magnitude for each galaxy, as measured within an aperture of 20 arcsec.

4.4 Internal comparisons and combination of photometric data

To assess the consistency of our photometric system from year-to-year, we have compared, for each galaxy in common, the mean derived aperture magnitude from the 1993 run, with that from the 1994 data. The comparison is shown in Figure 9, for apertures of 20 arcsec and 30 arcsec diameter. At 20 arcsec, the mean offset is 0.003 ± 0.002 mag, and the scatter 0.011 mag. The offset in the 30 arcsec aperture magnitudes, is 0.002 ± 0.004 mag, with a scatter of 0.020 mag. The increased scatter for the larger aperture results from the treatment of contaminating sources, companion galaxies, etc. We are confident, therefore, that our photometric system is internally consistent to better than 0.01 mag. Applying the same year-to-year test for D_n measurements, we find an offset between the runs of 0.000 ± 0.001 dex.

Since our photometric data are on the same system, we can combine repeated measurements of $\log D_n$, $\log A_e$ and $\langle \mu \rangle_e$, to give simple mean values. These are presented in Table 13 along with the spectroscopic parameters for each galaxy.

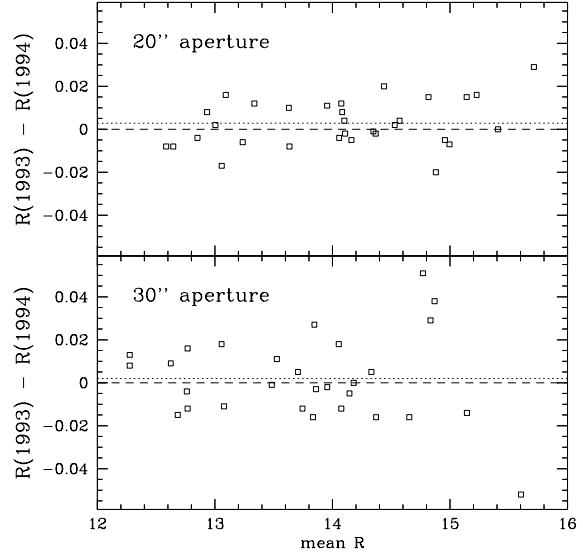
From a subset of 50 galaxies which have repeat observations, an estimate can be made of the typical uncertainty in our measurements of the photometric parameters. Figure 10 shows the comparison of these measurements. The scatter implies an error of 0.005 in each determination of $\log D_n$. For the FP parameters taken individually, the scatters are larger: 0.032 dex on A_e and 0.113 mag. arcsec⁻² on $\langle \mu \rangle_e$. The errors on these parameters are correlated, however. If we construct the quantity $\log A_e - 0.3 \langle \mu \rangle_e$, the combination often used to give an edge-on projection of the Fundamental Plane, we find that the uncertainty in this quantity is only 0.006, only slightly larger than that on $\log D_n$.

4.5 External comparisons

4.5.1 Aperture photometry

Figure 11 illustrates comparisons between our CCD aperture magnitudes, and R-band magnitudes tabulated by other authors, for galaxies in common. The comparisons are quantified in Table 9.

In the comparison with the photoelectric aperture photometry of Colless et al. (1993), we find a scatter which is well matched to the quadrature sum of our internal errors quoted above, and the similar uncertainties claimed by Colless et al. There exists, however, a small but significant offset of 0.037 mag. between the two datasets.

**Figure 9.** Year to year comparison of galaxy magnitudes, within apertures of 20 arcsec and 30 arcsec diameter. The dotted line represents the mean offset in each case. The scatter in the plot is 0.01 mag. at 20 arcsec aperture, and 0.02 mag. at 30 arcsec.

Between our study and that of Postman and Lauer (1995, PL) there are six galaxies in common, of which one is severely contaminated by a star. We use only the remaining five galaxies to derive the quoted offset. (In performing this comparison, we have corrected for the misidentification by PL of the A0262 brightest cluster galaxy with N0705, rather than N0708.)

Our data has been compared to the independent data of Steel (1997), which are also derived using the Harris R filter, but at a different telescope. The source of bimodality in this comparison has not been identified.

In conclusion, small zero-point discrepancies do exist at the level of a few 0.01 mag. between the present photometric system and data from the literature. Internally, however, the data presented here possess a consistency of better than 0.01 mag.

4.5.2 Derived parameters

Figure 12 and Table 10 present comparisons between the present data and photometric parameters from the literature, for galaxies in common. The comparison data are the R-band data of Steel (1997), the V-band measurements of Lucey et al. (1997), Gunn-r data from Jørgensen et al. (1995a), and B-band parameters from Burstein et al. (1987). For the comparison with Burstein et al., only measurements given quality code ‘1’ are included. The comparisons are performed for $\log D_n$ and for the FP combination, $\log A_e - 0.3 \langle \mu \rangle_e$. With the exception of the Burstein et al. data, the comparison galaxies are drawn entirely from the Coma cluster. The literature data are corrected for typical colours, according to the surface brightness level chosen by the author to define D_n . For instance, Jørgensen et al. define an r-band D_n at $\langle \mu \rangle_r = 19.60$ mag. arcsec⁻². Surface

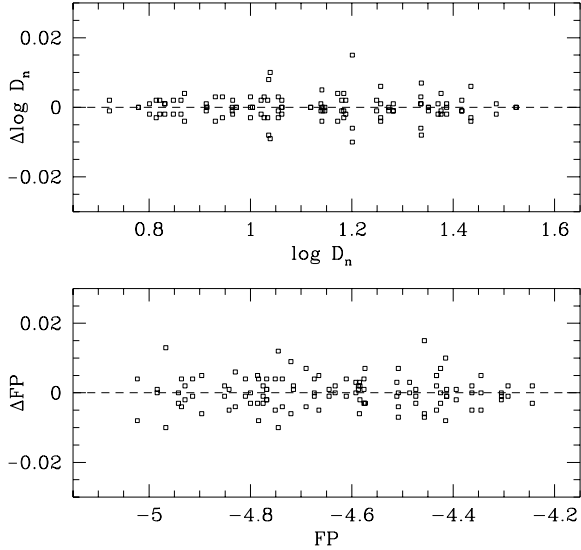


Figure 10. Upper panel : Scatter of repeat D_n measurements. For each galaxy with more than one observation, the individual measurements of $\log D_n$ are plotted against the mean value. Lower panel : Scatter of repeat measurements of the Fundamental Plane combination $\log A_e - 0.3\langle\mu\rangle_e$, denoted FP. (Note however, that the coefficient of $\langle\mu\rangle_e$ may not be precisely the same as for the FP distance indicator adopted in Paper II).

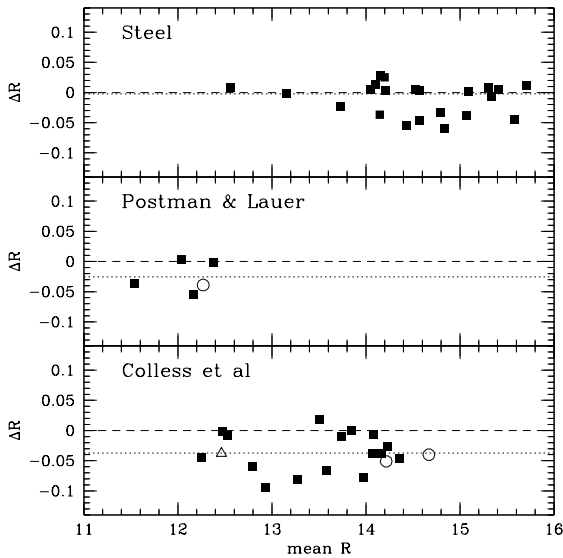


Figure 11. Comparison of our CCD aperture photometry with data from the literature. Upper panel : comparison with Steel (1997), at an aperture of 20 arcsec. Middle panel : comparison with Postman and Lauer (1995). The data used are for apertures of 63 arcsec (filled squares) and 79 arcsec (open circles). Lower panel : comparison with Colless et al. (1993), The comparison is performed for magnitudes within 19.2 arcsec (open circles), 29.9 arcsec (filled squares), 39.5 arcsec (open triangle). The comparisons are plotted in the sense ‘this work’ – ‘literature’. The dotted line indicates the mean offset in each case.

brightnesses from their paper are therefore corrected for a colour of 0.37 mag. in $r - R$.

The FP variables are compared in combination rather than separately, since the individual parameters $\log A_e$ and $\langle\mu\rangle_e$ can acquire correlated mean offsets from author to author, when the profile fit is performed over different ranges. The FP combination is, however, robust against changes to the range of fit.

The R-band photometry of Steel offers an independent validation of the present data, free from complications concerning band mis-matches, etc. The two samples agree to within 0.003 in both $\log D_n$ and the FP combination.

From the excellent agreement of the R-band D_n measurements, presented here, with the V-band data of Lucey et al., we justify, *a posteriori*, the definition of our R-band D_n diameter at $\langle\mu\rangle_R = 19.23$ mag. The slight trend may be a reflection of the $V - R$ colour–magnitude relation for the Coma cluster. The slope found here (converted to magnitudes) is -0.03 ± 0.01 , which may be compared with the $V - K$ colour–magnitude slope of -0.08 ± 0.01 reported by Bower et al. (1992). We note that the trend is in the expected sense, such that brighter galaxies are redder.

The D_n comparison with the Gunn-r data of Jørgensen et al. exhibits a curious bimodality. This is a result of their data being presented to only two decimal places in $\log D_n$ rather than three, as in our data. This is unfortunate, since their data is clearly more accurate than quoted, the dispersion given in Table 10 being consequently overestimated.

The significant offset found between this work and that of Jørgensen et al. is, of course, sensitive to the adopted $r - R$ colour. From a comparison of our aperture magnitudes with magnitudes predicted from their tabulated r-band parameters, we derive a mean $r - R$ colour of 0.33 mag. If a colour correction were applied based on this result, the offsets of between this work and that of Jørgensen et al. would be reduced to 0.004 ± 0.002 in $\log D_n$ and -0.006 ± 0.003 in the FP combination.

The photoelectric data of Burstein et al. have been corrected for the $(1+z)^4$ surface brightness dimming before comparison. The large offsets with respect to this source can be accounted for by the absence of a seeing correction in their data, as demonstrated by Jørgensen et al.

The scatter in the comparisons is sufficiently small that our D_n / FP measurements may be brought onto a system consistent with external CCD data, to within 0.003 dex in implied distance.

5 CONCLUSION

This paper has presented spectroscopic and photometric data to be used in a study of cluster peculiar motions in the Perseus–Pisces supercluster. The data comprise observations of 137 early-type galaxies in 9 clusters, and additional standard galaxies.

From intermediate-dispersion spectroscopy, the velocity dispersion σ has been derived for each galaxy, with a typical uncertainty of 7.6 per cent per measurement. The spectroscopic data also yield recession velocities (cz) (to an uncertainty of about 30 km s^{-1}), and Mg_2 indices (typical

Table 10. Comparison of new R-band photometric parameters with measurements from Steel (1997), Lucey et al. (1997), Jørgensen et al. (1995) and Burstein et al. (1987). For the Burstein et al. data, only measurements with quality code ‘1’ are included in the comparison. Offsets are corrected for assumed mean colours, *viz.* $\langle V - R \rangle = 0.57$, $\langle r - R \rangle = 0.37$, $\langle B - R \rangle = 1.52$.

Source	Parameter	N_{gal}	Mean Offset	Dispersion
Steel (1997) R-band	$\Delta(\log D_n)$	22	0.000 ± 0.001	0.007
	$\Delta(\log A_e - 0.3\langle\mu\rangle_e)$	22	-0.002 ± 0.001	0.008
Lucey et al. (1997) V-band	$\Delta(\log D_n)$	22	-0.003 ± 0.002	0.009
	$\Delta(\log A_e - 0.3\langle\mu\rangle_e)$	22	-0.001 ± 0.002	0.013
Jørgensen et al. (1995) r-band	$\Delta(\log D_n)$	22	-0.007 ± 0.002	0.009
	$\Delta(\log A_e - 0.3\langle\mu\rangle_e)$	22	-0.017 ± 0.002	0.014
Burstein et al. (1987) B-band	$\Delta(\log D_n)$	47	$+0.015 \pm 0.003$	0.025
	$\Delta(\log A_e - 0.3\langle\mu\rangle_e)$	31	$+0.022 \pm 0.004$	0.025

error 0.010 mag. per measurement). Extensive external comparisons are presented, allowing the σ and Mg_2 data to be placed onto a new ‘standard system’, with an uncertainty of less than 0.01 dex.

R-band CCD photometry is used to derive global photometric parameters. The photometric data comprise effective diameter (A_e), mean surface brightness within effective diameter ($\langle\mu\rangle_e$), and an R-band D_n parameter, defined analogously to the B-band photometric diameter of Dressler et al. (1987). The scatter of repeat observations indicates the following uncertainties – $\log A_e$: ± 0.032 ; $\langle\mu\rangle_e$: ± 0.113 ; $\log D_n$: ± 0.005 ; $\log A_e - 0.3\langle\mu\rangle_e$: ± 0.006 . The aperture magnitudes, from which the profile is determined, show systematic offsets (at the level of a few 0.01 mag) with respect to literature data. The derived $\log D_n$ and Fundamental Plane parameter ($\log A_e - 0.3\langle\mu\rangle_e$), show a typical scatter of ~ 0.010 with respect to similar data from the literature.

The scatter in the FP relation is ~ 0.08 dex, so that intrinsic scatter is dominant over random measurement errors. Currently, a major challenge in peculiar velocity work is to recognise and reduce the effects of *systematic* errors. We will defer until Paper II, a full discussion concerning such errors. For the present, we note that the high quality of the data presented here, together with the generous overlap secured with literature datasets, will allow us to address realistically the systematic errors in our peculiar velocity measurements.

ACKNOWLEDGMENTS

The Isaac Newton Telescope and Jacobus Kapteyn Telescope are operated on the island of La Palma by the Royal Greenwich Observatory in the Spanish Observatorio del Roque de los Muchachos of the Instituto de Astrofísica de Canarias. Data reduction was performed using Starlink facilities at Durham. JS and RJS acknowledge financial support from the PPARC. MJH acknowledges financial support from the PPARC; from a CITA National Fellowship; and from the Natural Sciences and Engineering Research Council of Canada, through operating grants to F. D. A. Hartwick and C. J. Pritchett. Alan Dressler is thanked for providing information for the subdivision of his Las Campanas datasets.

REFERENCES

- Andreon S. 1994 *A&A*, 284, 801
 Bower R.G., Lucey J.R., Ellis R.S. 1992, *MNRAS*, 254, 589
 Bucknell M.J., Godwin J.G., Peach J.V. 1979, *MNRAS*, 188, 579
 Burstein D., Heiles C. 1984, *ApJS*, 54, 33
 Burstein D., Davies R.L., Dressler A., Faber S.M., Stone R.P.S., Lynden-Bell D., Terlevich R.J., Wegner G. 1987, *ApJS*, 64, 601
 Chincarini G., Rood H.J. 1971, *ApJ*, 168, 321
 Colless M., Burstein D., Wegner G., Saglia R.P., McMahon R.K., Davies R.L., Bertschinger E., Baggle G. 1993, *MNRAS*, 262, 475
 Davies R.L., Burstein D., Dressler A., Faber S.M., Lynden-Bell D., Terlevich R.J., Wegner G. 1987, *ApJS*, 64, 581
 Dekel A. 1994, *ARA&A*, 32, 371
 Dressler A. 1980, *ApJ*, 236, 351
 Dressler A. 1984, *ApJ*, 281, 512
 Dressler A., Lynden-Bell D., Burstein D., Davies R.L., Burstein D., Faber S.M., Terlevich R.J., Wegner G. 1987, *ApJ*, 313, 42
 Dressler A., Faber S.M., Burstein D. 1991, *ApJ*, 368, 54
 Faber S.M., Wegner G., Burstein D., Davies R.L., Dressler A., Lynden-Bell D., Terlevich R.J. 1989, *ApJS*, 69, 763
 Frei Z., Gunn J.E. *AJ*, 108, 1476
 González J.J. 1993, PhD thesis, University of California, Santa Cruz
 Guzmán R., Lucey J.R., Carter D., Terlevich R.J. 1992, *MNRAS*, 257, 187
 Gregg M.D. 1995, *ApJ*, 443, 527
 Han M.-S., Mould J.R. 1992, *ApJ*, 396, 453
 Huchra J.P., Geller M.J., Clemens C.M., Tokarz S.P., Michel A. 1993, *Astronomical Data Center archives*
 Hudson M.J., 1993, *MNRAS*, 265, 43
 Hudson M.J., 1994, *MNRAS*, 266, 468
 Hudson M.J., Lucey J.R., Smith R.J., Steel J. 1997, *MNRAS*, submitted
 Irwin M., McMahon R. 1992, *Gemini (Newsletter of the Royal Greenwich Observatory)*, 37, 1
 Jackson R. 1982, Ph.D. thesis, University of California, Santa Cruz
 Jørgensen I, Franx M., Kjærgaard P. 1995a *MNRAS*, 273, 1097
 Jørgensen I, Franx M., Kjærgaard P. 1995b *MNRAS*, 276, 1341
 Jørgensen I, Franx M., Kjærgaard P. 1996 *MNRAS*, 280, 167
 Kolatt T., Dekel A. 1994, *ApJ*, 428, 35
 Landolt A.U. 1983, *AJ*, 88, 439
 Landolt A.U. 1992, *AJ*, 104, 340.
 Lucey J.R., Carter D. 1988, *MNRAS*, 235, 1177
 Lucey J.R., Gray P.M., Carter D., Terlevich R.J. 1991a, *MNRAS*, 248, 804

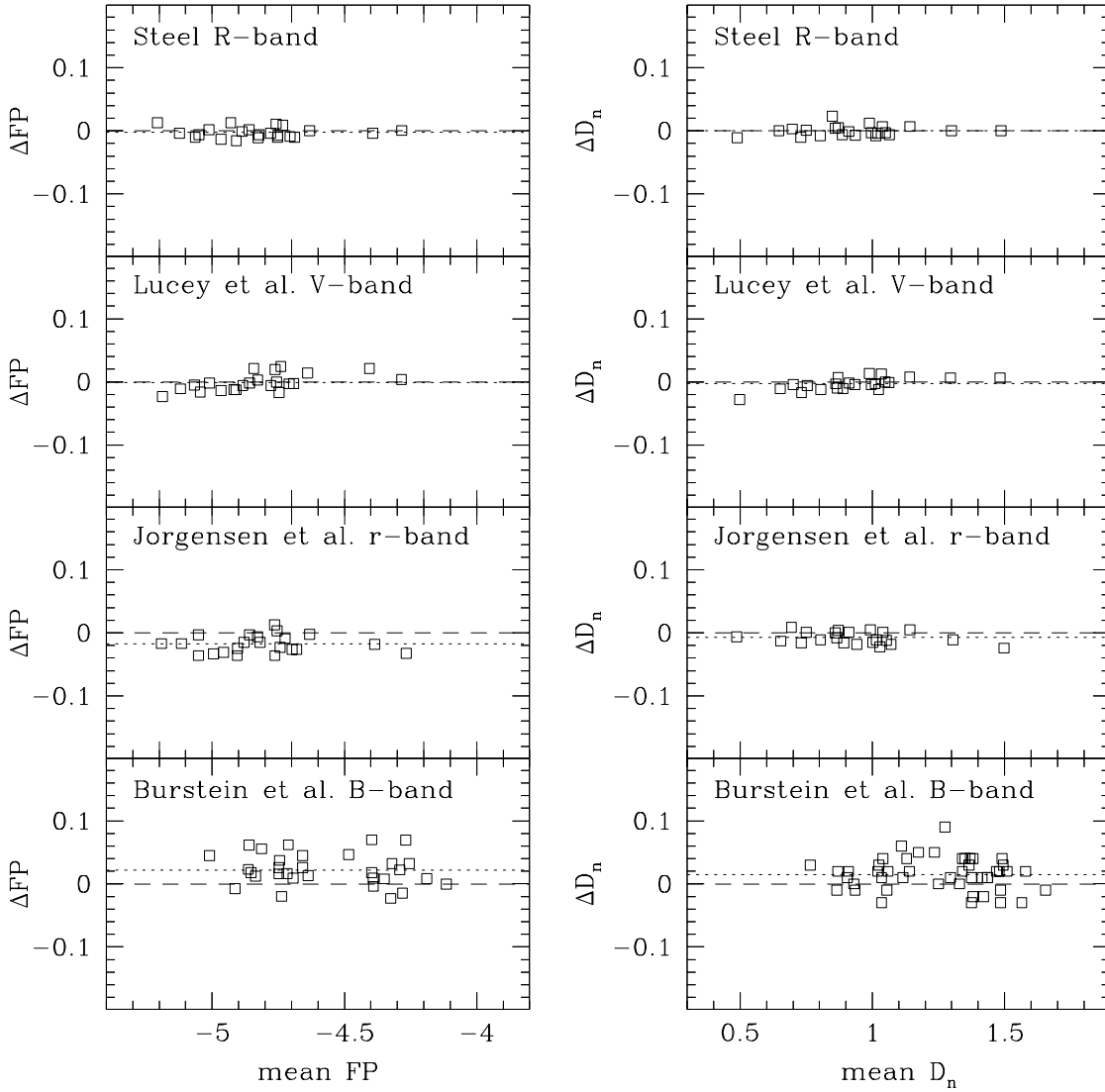


Figure 12. External comparisons of D_n and FP combination ($\log A_e - 0.3\langle\mu_e\rangle$). The comparison data are taken from Steel (1997) (R-band), Lucey et al. (1997) (V-band), Jørgensen et al. (1995b) (r-band) and Burstein et al. (1987) (B-band). ΔD_n and ΔFP are plotted in the sense ‘this work’ – ‘literature’, against the mean of our measurement and the literature value. The dotted line indicates the mean offset in each panel.

Lucey J.R., Guzmán R., Carter D., Terlevich R.J. 1991b, MNRAS, 253, 584

Lucey J.R., Guzmán R., Steel J., Carter D. 1994, in Cosmic Velocity Fields, ed. F. Bouchet & M. Lachièze-Rey, (Gif-sur-Yvette: Editions Frontières), p. 43

Lucey J.R., Guzmán R., Steel J., Carter D. 1997, MNRAS, 287, 899

Lucey J.R., Lahav O., Lynden-Bell D., Terlevich R.J., Infante, L., Melnick J. 1998, in preparation

Lynden-Bell D., Faber S.M., Burstein D., Davies R.L., Dressler A., Terlevich R.J., Wegner G. 1988, ApJ, 326, 19

Oke J.B., Sandage A. 1968, ApJ, 154, 21

Postman M., Lauer T.R. 1995, ApJ, 440, 28 (PL)

Poulain P., Nieto J.-L., Davoust E. 1991, A&AS, 95, 129

Saglia R.P., Bertschinger E., Baggle G., Burstein D., Colless

M.M., Davies R.L., McMahan R.K., Wegner G. 1997, ApJS, 109, 79

Sargent W.L.W., Schechter P.L., Boksenberk A., Shorridge K. 1977, ApJ, 212, 326

Saunders W. et al. 1991, Nature, 349, 32

Steel, J. 1997, Ph.D. thesis, University of Durham

Strauss M.A., Willick J.A. 1995 Physics Reports, 261, 271

Tully R.B., Fisher J.R. 1977, ApJ, A&A, 54, 661

Wegner G., Colless M., Baggle G., Davies R.L., Bertschinger E.,

Burstein D., McMahan R.K., Saglia R.P. 1996, ApJS, 106, 1

Willick J.A. 1990, ApJ, 352, L45

Willick J.A. 1991, PhD thesis, University of California, Berkeley

Willick J.A., Courteau S., Faber S.M., Burstein D., Dekel A.,

Strauss M.A. 1997, ApJS, 109, 333

Table 11. Raw spectroscopic data. In addition to our reference number for each galaxy, we tabulate under ‘Other ID’ the relevant number from NGC, IC, UGC, CGCG catalogues, or from other published work. For each individual observation we list: the dataset from which values derive; cz = heliocentric recession velocity; σ = central velocity dispersion (kms^{-1}); ε_σ = poisson error on σ ; Mg_2 = magnesium index (magnitudes) and $\varepsilon_{\text{Mg}_2}$ = Poisson error on Mg_2 .

Our ID	Other ID	Dataset	cz	σ	ε_σ	Mg_2	$\varepsilon_{\text{Mg}_2}$
Cluster : 7S21							
S01	N0079	TEK94	5479	194	11	0.307	0.012
S02	N0085A	TEK94	6189	108	6	0.239	0.012
S03	N0083	TEK94	6263	253	14	0.321	0.013
		TEK94	6262	253	16	-	-
S04	N0080	TEK94	5748	261	12	0.300	0.010
		TEK94	5734	249	13	0.305	0.009
S05	I1548	TEK94	5775	149	6	0.197	0.008
S06	-	TEK94	5637	127	7	0.206	0.013
		TEK94	5655	131	13	-	-
S07	CGCG457-008	TEK94	5926	115	8	0.254	0.012
Cluster : Pisces							
Z01026	N0398	TEK94	4912	104	6	0.261	0.009
Z01027	N0379	TEK94	5503	225	10	0.298	0.009
		EEV93	5492	243	16	0.287	0.012
Z01030	N0380	EEV93	4448	314	12	0.329	0.007
		TEK94	4452	308	19	0.343	0.012
		EEV93	4441	337	15	0.328	0.009
		TEK94	4398	272	10	0.328	0.007
		TEK94	4442	301	11	0.343	0.007
Z01032	-	EEV93	4753	104	9	0.262	0.015
Z01034	CGCG501-077	EEV93	5151	115	11	0.258	0.013
		TEK94	5152	127	5	0.267	0.008
Z01035	N0383	EEV93	5082	269	11	0.293	0.008
		TEK94	5084	269	11	0.314	0.007
		EEV93	5009	249	22	0.299	0.014
		TEK94	5154	314	13	0.306	0.009
		TEK94	5117	316	18	-	-
Z01035C1	N0382	EEV93	5243	222	10	0.275	0.009
		TEK94	5240	202	8	0.277	0.008
		EEV93	5233	195	16	0.246	0.015
		TEK94	5265	200	10	0.273	0.010
Z01036	I1618	EEV93	4720	90	9	0.214	0.017
Z01041	N0386	EEV93	5563	145	9	0.248	0.012
		TEK94	5548	121	7	0.247	0.011
Z01043	N0375	EEV93	5910	180	10	0.265	0.010
Z01045	N0385	EEV93	4988	198	8	0.271	0.009
		TEK94	5024	210	9	0.295	0.008
		TEK94	5027	195	10	-	-
Z01046	N0388	TEK94	5473	148	8	0.251	0.009
		EEV93	5445	121	9	0.251	0.013
Z01047	-	TEK94	5493	132	6	0.285	0.009
Z01049	N0384	EEV93	4255	257	10	0.309	0.009
		TEK94	4258	275	10	0.313	0.008
		EEV93	4267	245	12	0.291	0.010
Z01073	CGCG501-102	EEV93	5174	172	10	0.276	0.011
		TEK94	5169	149	8	0.273	0.010
Z02057	N0420	EEV93	5038	196	13	0.229	0.011
		TEK94	5005	179	7	0.250	0.007
Z04035	-	EEV93	23995	261	17	0.238	0.013
Z04049	N0394	EEV93	4378	172	7	0.253	0.010
		TEK94	4404	195	8	0.260	0.008
		EEV93	4364	178	10	0.274	0.009
Z04050	N0392	EEV93	4684	234	8	0.291	0.008
		TEK94	4665	231	7	0.292	0.006
		EEV93	4668	239	10	0.301	0.007
Z04051	N0397	TEK94	4988	124	8	0.258	0.009
Z05034	I1638	EEV93	4810	141	8	0.256	0.010
		TEK94	4814	162	7	0.276	0.008
		TEK94	4868	142	7	0.277	0.009
		TEK94	4811	137	7	0.278	0.010
Z05044	I1648	TEK94	5541	124	8	0.266	0.010
Z05052	N0410	EEV93	5315	292	11	0.344	0.007
		TEK94	5327	301	11	0.350	0.007
		TEK94	5309	310	12	0.346	0.007
		TEK94	5295	300	13	-	-
Z10020	-	TEK94	4852	85	7	0.227	0.013

Table 11 – continued

Our ID	Other ID	Dataset	cz	σ	ε_σ	Mg_2	ε_{Mg_2}
Z14028	CGCG501-070	TEK94	4264	206	8	0.328	0.008
		EEV93	4252	192	10	0.307	0.009
Z16012	-	TEK94	17740	163	15	0.268	0.015
Z17005	-	TEK94	4651	105	6	0.205	0.010
Cluster : HMS0122+3305							
H01022	N0528	EEV94	4806	245	9	-	-
H01027	-	TEK94	4976	99	9	0.210	0.011
H01041	N0499	EEV94	4387	267	13	-	-
		TEK94	4399	259	10	0.327	0.006
H01044	N0501	TEK94	5010	163	15	0.304	0.011
H01051	CGCG502-043	EEV94	5225	153	9	-	-
		TEK94	5246	117	7	0.266	0.011
H01056	I1680	TEK94	4438	136	6	0.267	0.010
H01057	N0508	EEV94	5505	225	13	-	-
		TEK94	5526	228	12	0.310	0.009
H01064	N0507	EEV94	4936	306	15	-	-
		TEK94	4937	290	11	0.299	0.006
		TEK94	4934	295	7	0.294	0.006
H01075	CGCG502-044	TEK94	5141	133	8	0.278	0.009
H01078	I1673	TEK94	5090	190	7	0.275	0.008
H04010	N0529	EEV94	4815	236	9	-	-
		TEK94	4773	239	8	0.295	0.006
Cluster : A0262							
A01043	N0687	EEV93	5112	204	10	0.276	0.011
		TEK94	5091	247	8	0.306	0.006
A01047	CGCG522-048	TEK94	4151	144	7	0.263	0.008
A01067	N0703	TEK94	5580	225	8	0.311	0.008
A01069	N0708	TEK94	4855	219	16	0.321	0.016
		TEK94	4874	230	18	0.316	0.013
A01071	N0705	EEV93	4514	183	12	0.258	0.011
A01074	N0704	EEV93	4709	161	10	0.296	0.013
		TEK94	4730	159	6	0.275	0.007
A01076	-	EEV93	4284	125	13	0.275	0.020
		TEK94	4274	128	7	0.261	0.011
A01094	-	TEK94	14620	266	19	0.290	0.012
A02025	N0759	EEV93	4667	259	14	0.247	0.011
		TEK94	4601	261	17	0.250	0.008
A05096	CGCG522-089	TEK94	5245	92	10	0.220	0.014
A05106	N0732	EEV93	5894	141	11	0.185	0.013
A09029	I0171	EEV93	5360	173	11	0.227	0.012
		TEK94	5392	208	10	0.266	0.009
A14050	-	TEK94	5147	140	10	0.236	0.016
A14078	N0679	TEK94	5049	254	9	0.305	0.007
A19041	U01269	TEK94	3867	129	11	0.175	0.013
		TEK94	3829	105	9	0.195	0.012
Cluster : A0347							
B02	U01837	TEK94	6582	197	13	0.302	0.012
B03	U01841	TEK94	6373	235	15	0.304	0.011
B03C	-	TEK94	6649	303	18	0.305	0.011
B06	U01859	TEK94	5917	362	17	0.349	0.009
B07	CGCG538-065	TEK94	5301	207	10	0.309	0.008
B08	N909	TEK94	4978	191	12	0.271	0.009
B09	N910	TEK94	5253	259	12	0.326	0.010
		TEK94	5222	243	13	0.342	0.010
B10	N911	TEK94	5766	256	16	0.323	0.011
B11	N912	TEK94	4418	175	9	0.290	0.010
B16	CGCG539-042	TEK94	4885	156	7	0.267	0.010
Cluster : J8							
J01049	CGCG483-070	EEV93	8555	316	24	0.298	0.012
		TEK94	8557	312	17	0.308	0.009
		EEV93	8556	299	34	0.298	0.015
J01055	-	TEK94	9613	143	13	0.283	0.020
		TEK94	9620	162	14	0.276	0.019
J01056	CGCG483-068	EEV93	9438	212	17	0.333	0.016
		TEK94	9544	228	12	0.307	0.012
		TEK94	9549	253	13	0.316	0.011
J01060	I1803	TEK94	9583	366	13	0.337	0.007
J01065	-	TEK94	9103	133	10	0.153	0.010
J01067	EFAR-J8-I	TEK94	9233	199	11	0.301	0.012
		EEV93	9232	197	21	0.290	0.017

Table 11 – *continued*

Our ID	Other ID	Dataset	<i>cz</i>	σ	ε_σ	Mg ₂	$\varepsilon_{\text{Mg}_2}$
J01069	I1807	TEK94	9094	199	9	0.266	0.009
		EEV93	9013	208	14	0.252	0.014
J01070	I1806	EEV93	10190	177	23	0.306	0.017
		TEK94	10211	219	11	0.296	0.011
		EEV93	10236	245	24	0.286	0.018
J01080	-	TEK94	9731	164	12	0.240	0.012
J03049	-	EEV93	9929	264	27	0.244	0.017
		TEK94	9927	242	19	0.265	0.011
J06039	CGCG484-006	TEK94	4268	135	5	0.273	0.007
J07038	-	TEK94	10136	182	11	0.269	0.012
J08035	-	TEK94	10099	81	11	0.167	0.017
J08036	EFAR-J8-K	EEV93	9770	170	16	0.278	0.018
		TEK94	9802	204	11	0.283	0.010
		EEV93	9817	196	14	0.267	0.018
J09035	-	TEK94	11133	282	17	0.325	0.010
Cluster : Perseus (A0426)							
P01	I0293	EEV93	4704	150	11	0.260	0.015
P02	N1224	TEK94	5235	247	10	0.270	0.009
P03	I0310	TEK94	5660	218	12	0.249	0.010
P05	I0312	EEV93	4978	222	13	0.296	0.012
P07	CR19	TEK94	3544	123	10	0.239	0.015
P08	CR20	TEK94	6454	188	13	0.271	0.017
		TEK94	6469	215	11	0.259	0.012
P11	BGP44	TEK94	4247	159	14	0.275	0.014
P12	N1270	EEV93	4965	351	16	0.350	0.010
		TEK94	5019	341	14	0.355	0.008
P13	PER195	TEK94	8391	163	7	0.275	0.009
		EEV93	8392	193	20	0.283	0.018
P14	PER199	EEV93	5078	226	16	0.275	0.016
		TEK94	5105	210	14	0.290	0.016
		TEK94	5113	213	7	0.279	0.008
P15	CR28	TEK94	6213	212	7	0.288	0.009
P16	CR27	EEV93	8053	171	13	0.266	0.012
P17	N1272	TEK94	3802	272	16	0.331	0.011
		EEV93	3815	270	20	0.344	0.013
		EEV93	3794	286	20	0.340	0.013
		TEK94	3791	240	14	0.342	0.011
		EEV93	3801	278	15	0.334	0.014
		EEV94	3777	276	24	-	-
		TEK94	3794	263	11	0.338	0.011
P18	N1273	EEV93	5387	207	15	0.249	0.013
P19	I1907	EEV93	4479	195	18	0.278	0.016
P20	BGP111	TEK94	3963	86	8	0.279	0.020
P21	PER152	TEK94	3937	142	9	0.309	0.015
		TEK94	3943	136	9	0.315	0.014
P22	CR36	EEV93	7460	202	14	0.280	0.012
P23	N1278	EEV93	6044	238	15	0.292	0.011
		EEV94	6074	277	19	-	-
		TEK94	6061	270	14	0.306	0.011
P26	BGP59	TEK94	5315	207	9	0.283	0.010
P27	U02673	EEV93	4424	197	14	0.288	0.013
P28	N1281	TEK94	4300	276	12	0.324	0.010
P29	N1282	TEK94	2210	213	7	0.292	0.009
		EEV93	2223	203	11	0.290	0.012
		EEV93	2226	210	14	0.264	0.012
		TEK94	2216	228	9	0.277	0.009
P30	N1283	EEV93	6744	224	12	0.277	0.012
		EEV94	6735	204	13	-	-
P31	PER163	TEK94	5483	200	11	0.293	0.013
		TEK94	5480	164	7	0.278	0.008
P33	BGP33	TEK94	4950	168	8	0.289	0.009
P34	I0313	TEK94	4432	242	11	0.331	0.009
P36	N1293	EEV93	4170	216	12	0.293	0.011
		EEV93	4149	218	23	0.307	0.015
		TEK94	4164	208	8	0.319	0.008
P37	U02698	EEV93	6472	373	22	0.318	0.012
		TEK94	6421	364	14	0.340	0.009
P38	U02717	EEV93	3778	165	13	0.239	0.015
		TEK94	3798	153	9	0.227	0.011
P39	U02725	TEK94	6215	220	10	0.293	0.008

Table 11 – continued

Our ID	Other ID	Dataset	<i>cz</i>	σ	ε_σ	Mg ₂	$\varepsilon_{\text{Mg}_2}$
Cluster : Coma (A1656)							
N4875	COMA-D104	EEV93	8047	168	13	0.272	0.014
N4886	COMA-D151	EEV93	6372	167	8	0.252	0.014
N4860	COMA-D194	EEV93	7944	312	27	0.324	0.015
N4881	COMA-D217	EEV93	6732	166	14	0.270	0.016
I4011	COMA-D150	EEV93	7233	118	13	0.260	0.024
COMA-D125	-	EEV93	6910	174	19	0.232	0.017
Cluster : A2199							
A21-F113	-	TEK94	7995	169	14	0.242	0.016
		TEK94	8068	163	12	0.263	0.013
		TEK94	8017	170	9	0.254	0.012
		TEK94	8128	158	15	0.262	0.013
A21-F114	-	TEK94	9177	199	12	0.294	0.013
		TEK94	9179	212	12	0.288	0.011
		TEK94	9128	191	10	0.278	0.010
		TEK94	9255	192	9	0.300	0.010
A21-F121	A2199-S26	TEK94	8783	177	15	0.270	0.013
		TEK94	8754	170	11	0.278	0.012
A21-F144	A2199-S30	TEK94	8510	256	12	0.244	0.010
		TEK94	8539	259	9	0.254	0.008
A21-F145	-	TEK94	7586	152	8	0.270	0.012
		TEK94	7634	146	8	0.282	0.010
A21-F146	A2199-S34	TEK94	8302	158	9	0.263	0.014
		TEK94	8327	163	11	0.254	0.011
A21-F164	N6166	TEK94	9329	269	25	0.321	0.014
		TEK94	9367	285	18	0.298	0.011
A21-Z34A	A2199-Z34A	TEK94	8724	208	10	0.260	0.008
		TEK94	8718	190	9	0.289	0.009
A21-Z34AC	-	TEK94	8949	227	9	0.297	0.008
		TEK94	8980	208	8	0.325	0.009
N6158	-	TEK94	8936	197	14	0.272	0.015
		TEK94	8925	186	9	0.264	0.011
		TEK94	8963	174	7	0.280	0.008
Cluster : A2634							
A26-F102	A2634-D107	TEK94	9298	213	13	-	-
A26-F1201	A2634-D79	TEK94	10156	188	12	0.272	0.014
		EEV93	10166	118	10	0.298	0.017
		EEV93	10178	146	21	0.270	0.023
		TEK94	10144	169	11	0.275	0.013
A26-F121	A2634-D80	TEK94	9547	206	16	0.284	0.014
		EEV93	9571	157	13	0.250	0.016
		EEV93	9595	163	20	0.257	0.023
		TEK94	9595	186	12	0.270	0.013
A26-F1221	N7720	EEV93	9117	354	23	0.308	0.010
		TEK94	9110	322	16	0.322	0.010
		TEK94	9105	340	16	0.310	0.009
		EEV93	9091	310	16	0.305	0.009
		TEK94	9079	349	15	0.320	0.007
A26-F1222	A2634-D76	EEV93	8107	230	15	0.276	0.013
		TEK94	8091	209	13	0.278	0.013
		TEK94	8143	176	14	0.289	0.012
		EEV93	8139	209	11	0.274	0.013
		TEK94	8115	230	15	0.275	0.009
A26-F129	A2634-D74	EEV93	8423	199	16	0.267	0.015
		TEK94	8420	213	11	0.289	0.010
		TEK94	8422	202	10	0.290	0.011
A26-F134	A2634-D55	EEV93	9281	221	14	0.279	0.012
		TEK94	9287	232	10	0.284	0.008
		TEK94	9286	206	11	0.287	0.009
A26-F138	A2634-D58	EEV93	10883	240	18	0.287	0.012
		TEK94	10849	221	13	0.295	0.012
		TEK94	10924	220	12	0.316	0.011
		EEV93	10815	195	22	0.287	0.022
A26-F139	A2634-D57	EEV93	9604	206	11	0.300	0.012
		TEK94	9563	212	13	0.309	0.012
		TEK94	9633	216	11	0.335	0.011
		EEV93	9545	217	26	0.277	0.021
A26-F1482	A2634-D38	TEK94	9345	240	22	-	-

Table 11 – *continued*

Our ID	Other ID	Dataset	cz	σ	ε_σ	Mg_2	ε_{Mg_2}
Field and standards							
N0541	-	TEK94	5443	218	13	0.307	0.010
N0545	-	TEK94	5341	244	10	0.303	0.008
N0547	-	TEK94	5545	250	12	0.314	0.008
N0548	-	TEK94	5410	148	8	0.237	0.011
N0584	-	TEK94	1833	205	11	0.291	0.009
		TEK94	1830	196	7	0.267	0.007
N0596	-	TEK94	1872	162	5	0.251	0.006
N0621	U01147	EEV93	5086	198	12	0.273	0.013
N0661	U01215	EEV93	3827	197	7	0.288	0.008
		EEV94	3817	186	6	-	-
N0680	U01286	EEV93	2963	210	8	0.279	0.008
		EEV94	2917	196	8	-	-
N0741	-	TEK94	5545	264	23	0.343	0.029
N0770	U01463	EEV93	2569	111	10	0.213	0.012
		EEV94	2505	126	9	-	-
N0821	-	TEK94	1753	208	6	0.316	0.009
		TEK94	1758	196	13	0.304	0.014
N0936	-	TEK94	1439	205	8	0.302	0.008
		EEV94	1306	182	9	-	-
		TEK94	1331	183	12	0.300	0.014
N0968	U02040	EEV93	3627	217	11	0.267	0.011
		EEV94	3599	201	9	-	-
N1023	-	EEV93	614	194	18	0.326	0.014
		EEV93	622	205	10	0.324	0.009
N1198	U02533	EEV93	1592	74	6	0.113	0.008
N3377	-	EEV93	655	174	7	0.274	0.006
		EEV93	679	129	7	0.266	0.007
N3379	-	EEV93	896	216	5	0.313	0.004
N3384	-	EEV93	735	171	4	0.310	0.006
N3412	-	EEV93	857	104	4	0.238	0.007
N3489	-	EEV93	690	96	4	0.188	0.005
N3862	-	EEV93	6498	258	15	0.297	0.013
N4472	-	EEV93	966	270	18	0.307	0.017
N4478	-	EEV93	1356	159	11	0.270	0.022
N4564	-	EEV93	1158	191	19	0.380	0.015
N6173	-	TEK94	8790	292	13	0.295	0.007
		TEK94	8870	279	16	0.287	0.010
N6411	-	TEK94	3756	192	13	0.277	0.011
		TEK94	3845	175	8	0.269	0.009
N6482	-	TEK94	3841	304	12	0.333	0.009
		TEK94	3931	295	14	0.329	0.016
N6702	-	TEK94	4761	196	12	0.263	0.013
		TEK94	4748	169	9	0.262	0.011
		TEK94	4739	177	16	0.293	0.012
N6703	-	TEK94	2393	190	12	0.281	0.010
		TEK94	2408	201	8	0.265	0.007
		TEK94	2388	195	7	0.281	0.007
N7236	-	TEK94	7879	247	10	0.270	0.008
N7237	-	TEK94	7868	203	11	0.312	0.014
N7385	-	TEK94	7856	282	15	0.321	0.009
N7391	-	TEK94	3048	259	9	0.324	0.009
N7454	-	TEK94	2058	105	6	0.202	0.010
		TEK94	1988	99	8	-	-
N7562	-	TEK94	3657	250	12	0.277	0.009
N7617	-	TEK94	4172	130	8	0.217	0.013
N7619	-	TEK94	3814	337	12	0.335	0.007
		EEV94	3836	338	14	-	-
N7626	-	TEK94	3425	281	13	0.322	0.010
		EEV94	3454	274	7	-	-
N7768	-	TEK94	8179	339	14	0.299	0.008
I2955	-	EEV93	6478	245	20	0.228	0.019
U02554	-	TEK94	2863	135	19	0.261	0.017
U03115	-	TEK94	3255	120	18	0.119	0.021
Q05	CGCG477-023	TEK94	8432	204	11	0.296	0.010

Table 12. Photometric data. Together with identification numbers, we tabulate: R_{20} = raw magnitude within 20 arcsec diameter aperture; A_B = B-band galactic extinction; psf = FWHM seeing (arcsec), as measured from stellar images; $\log A_e$ = log effective diameter (arcsec); $\langle \mu \rangle_e$ = mean surface brightness (mag. arcsec $^{-2}$) within A_e ; rms = rms residual of galaxy profile to best-fit $R^{1/4}$ law (magnitudes); $\log D_n$ = log R-band photometric D_n parameter (arcsec).

Our ID	Other ID	R_{20}	A_B	psf	$\log A_e$	$\langle \mu \rangle_e$	rms	$\log D_n$
Cluster : 7S21								
S01	N0079	13.69	0.05	1.8	1.354	20.00	0.01	1.132
S02	N0085A	14.16	0.05	1.5	1.502	20.99	0.03	0.953
S03	N0083	13.10	0.09	1.5	1.659	20.43	0.04	1.318
S04	N0080	12.95	0.09	1.6	1.691	20.28	0.04	1.364
S05	I1548	14.04	0.09	1.2	0.992	18.91	0.03	1.072
S06	-	14.88	0.09	1.0	1.128	20.34	0.01	0.796
S07	CGCG457-008	14.07	0.11	1.3	1.128	19.47	0.02	1.055
Cluster : Pisces								
Z01026	N0398	14.10	0.18	1.1	1.155	19.63	0.01	1.046
Z01027	N0379	12.92	0.17	1.2	1.518	19.81	0.07	1.380
		12.94	0.17	1.5	1.509	19.79	0.06	1.375
		12.94	0.17	1.2	1.600	20.06	0.05	1.374
Z01030	N0380	12.86	0.17	1.1	1.341	19.03	0.03	1.385
		12.85	0.17	1.5	1.307	18.90	0.02	1.387
		12.85	0.17	1.2	1.309	18.90	0.02	1.388
Z01032	-	14.78	0.18	2.0	1.100	20.08	0.01	0.852
Z01034	CGCG501-077	14.19	0.16	1.0	1.192	19.79	0.04	1.026
Z01035	N0383	12.59	0.17	1.0	1.788	20.27	0.04	1.483
		12.58	0.17	1.2	1.791	20.27	0.04	1.486
Z01035C1	N0382	13.64	0.17	1.0	1.093	18.93	0.04	1.186
		13.63	0.17	1.2	1.079	18.87	0.04	1.190
Z01036	I1618	14.32	0.16	1.2	1.242	20.16	0.02	0.967
		14.34	0.16	2.7	1.252	20.21	0.02	0.963
Z01041	N0386	14.11	0.17	1.0	1.042	19.25	0.06	1.044
		14.16	0.17	0.8	1.107	19.54	0.05	1.028
Z01043	N0375	14.27	0.17	0.8	0.840	18.50	0.01	1.035
Z01045	N0385	13.33	0.17	1.1	1.408	19.72	0.02	1.258
		13.31	0.17	0.7	1.409	19.70	0.02	1.263
		13.35	0.17	1.4	1.380	19.65	0.02	1.253
		13.34	0.17	1.4	1.386	19.66	0.02	1.254
Z01046	N0388	14.22	0.18	0.8	0.905	18.72	0.02	1.049
		14.28	0.18	1.7	0.857	18.61	0.03	1.030
Z01047	-	14.44	0.17	0.8	0.839	18.66	0.01	0.991
Z01049	N0384	13.24	0.17	1.1	1.187	18.88	0.02	1.281
		13.24	0.17	1.4	1.171	18.82	0.01	1.281
		13.23	0.17	1.4	1.212	18.95	0.02	1.283
Z01073	CGCG501-102	14.08	0.18	1.1	1.072	19.22	0.04	1.060
		14.07	0.18	1.2	1.050	19.11	0.04	1.064
Z02057	N0420	13.08	0.16	1.1	1.523	19.87	0.02	1.330
		13.06	0.16	1.5	1.542	19.90	0.03	1.337
		13.06	0.16	1.6	1.539	19.90	0.02	1.337
		13.05	0.16	1.2	1.521	19.83	0.02	1.339
Z04049	N0394	13.61	0.18	1.1	1.074	18.82	0.01	1.188
		13.64	0.18	1.8	1.011	18.62	0.03	1.183
		13.63	0.18	1.4	1.070	18.83	0.01	1.181
Z04050	N0392	13.00	0.18	1.1	1.366	19.26	0.02	1.351
		13.01	0.18	1.8	1.382	19.32	0.02	1.351
		13.01	0.18	1.4	1.373	19.29	0.02	1.350
Z04051	N0397	14.36	0.18	1.0	1.005	19.25	0.01	0.997
		14.34	0.18	1.8	1.032	19.32	0.02	1.003
		14.35	0.18	1.4	1.011	19.26	0.02	1.000
Z05034	I1638	13.80	0.16	1.1	1.236	19.60	0.03	1.119
		13.80	0.16	1.4	1.252	19.66	0.03	1.119
Z05044	I1648	14.07	0.17	1.7	1.116	19.47	0.03	1.050
Z05052	N0410	12.50	0.19	0.8	1.732	19.93	0.02	1.524
		12.50	0.19	1.7	1.737	19.93	0.03	1.524
Z10020	CGCG501-126	14.62	0.20	1.4	1.134	20.08	0.03	0.879
Z14028	CGCG501-070	13.78	0.18	1.2	0.928	18.39	0.02	1.143
		13.80	0.18	1.6	0.928	18.40	0.01	1.142
Z16012	-	15.36	0.14	1.3	0.941	19.80	0.01	0.779
Z17005	-	14.47	0.17	1.5	0.937	19.14	0.03	0.969
Cluster : HMS0122+3305								
H01022	N0528	13.05	0.17	1.2	1.330	19.20	0.01	1.338
H01041	N0499	12.55	0.17	1.2	1.545	19.44	0.01	1.481
H01044	N0501	14.14	0.16	1.2	1.029	19.16	0.02	1.041
H01051	CGCG502-043	14.08	0.13	1.1	1.100	19.41	0.01	1.048
H01056	I1680	14.03	0.17	1.1	1.035	19.05	0.03	1.073

Table 12 – *continued*

Our ID	Other ID	R_{20}	A_B	psf	$\log A_e$	$(\mu)_e$	rms	$\log D_n$
H01057	N0508	13.43	0.16	1.0	1.445	19.96	0.02	1.224
H01064	N0507	12.48	0.16	1.0	1.668	19.70	0.05	1.512
H01078	I1673	13.81	0.13	1.0	0.856	18.14	0.01	1.139
H04010	N0529	12.64	0.15	1.1	1.424	19.14	0.01	1.448
Cluster : A0262								
A01043	N0687	12.79	0.21	1.2	1.478	19.41	0.02	1.420
A01047	CGCG522-048	13.86	0.24	1.1	1.327	19.95	0.03	1.104
A01067	N0703	13.47	0.24	1.8	1.361	19.69	0.01	1.233
A01069	N0708	13.27	0.24	1.8	2.095	21.75	0.05	1.282
A01071	N0705	13.57	0.24	1.8	1.181	19.19	0.04	1.209
A01074	N0704	13.76	0.24	1.7	1.153	19.22	0.01	1.155
A01076	-	14.55	0.24	1.7	1.154	20.02	0.02	0.931
A01094	-	14.66	0.18	1.1	1.030	19.48	0.02	0.955
A02025	N0759	12.99	0.20	1.1	1.543	19.85	0.01	1.363
A05096	CGCG522-089	14.59	0.18	1.1	1.290	20.55	0.03	0.897
A09029	I0171	12.90	0.20	1.4	1.777	20.47	0.02	1.407
A19041	U01269	14.32	0.13	1.3	1.479	21.05	0.01	0.910
Cluster : A0347								
B02	U01837	13.52	0.34	1.4	1.589	20.43	0.01	1.234
B03	U01841	13.18	0.34	1.4	1.826	20.77	0.02	1.344
		13.22	0.34	1.4	1.799	20.74	0.02	1.329
B03C	-	14.51	0.34	1.4	0.575	17.45	0.01	1.030
		14.52	0.34	1.4	0.601	17.57	0.00	1.024
B06	U01859	13.20	0.31	1.4	1.182	18.68	0.02	1.321
B07	CGCG538-065	13.66	0.39	1.5	1.200	19.20	0.01	1.203
B08	N909	13.48	0.27	1.2	1.284	19.36	0.03	1.235
B09	N910	13.42	0.27	1.4	2.025	21.66	0.01	1.227
B10	N911	13.21	0.27	1.5	1.206	18.81	0.02	1.312
B11	N912	13.81	0.24	1.2	1.219	19.52	0.01	1.138
B16	CGCG539-042	13.88	0.30	1.6	1.336	19.94	0.03	1.120
Cluster : J8								
J01049	CGCG483-070	13.93	0.31	1.5	1.164	19.32	0.01	1.136
J01055	-	14.43	0.28	1.4	1.917	22.31	0.02	0.829
		14.46	0.28	2.2	1.909	22.29	0.01	0.832
		14.44	0.28	1.9	1.920	22.31	0.01	0.832
J01056	CGCG483-068	14.08	0.31	1.4	1.667	21.14	0.03	1.058
		14.09	0.31	2.2	1.701	21.25	0.04	1.052
		14.08	0.31	1.9	1.717	21.29	0.04	1.054
J01060	I1803	13.43	0.28	1.8	1.278	19.22	0.02	1.273
J01065	-	14.83	0.28	2.0	0.856	19.01	0.01	0.912
		14.82	0.28	1.0	0.829	18.90	0.02	0.914
J01067	EFAR-J8-I	14.65	0.28	3.0	1.205	20.18	0.03	0.920
J01069	I1807	14.19	0.31	2.0	1.118	19.44	0.03	1.062
J01070	I1806	14.37	0.31	2.4	1.299	20.22	0.01	1.004
		14.37	0.31	1.8	1.290	20.20	0.01	1.004
J01080	-	15.09	0.34	1.8	0.869	19.28	0.01	0.855
J03049	-	14.11	0.28	2.2	1.431	20.48	0.01	1.062
		14.11	0.28	1.6	1.445	20.53	0.02	1.062
J07038	-	15.07	0.32	2.4	0.991	19.74	0.01	0.846
		15.06	0.32	1.0	0.995	19.74	0.01	0.850
J08035	-	15.24	0.33	1.9	0.993	20.04	0.09	0.724
		15.24	0.33	2.0	1.254	20.95	0.04	0.721
J08036	EFAR-J8-K	14.53	0.33	1.9	1.215	20.06	0.02	0.972
		14.53	0.33	2.0	1.197	19.99	0.02	0.972
J09035	-	14.84	0.35	2.0	1.143	20.01	0.05	0.915
Cluster : Perseus (A0426)								
P01	I0293	13.93	0.56	0.9	1.597	20.76	0.03	1.114
P02	N1224	13.34	0.56	1.0	1.455	19.71	0.01	1.322
P03	I0310	13.20	0.60	1.0	1.628	20.06	0.01	1.377
P05	I0312	13.49	0.76	1.2	1.399	19.58	0.03	1.310
P07	CR19	14.69	0.65	1.3	1.336	20.61	0.02	0.912
P08	CR20	13.70	0.65	1.3	1.482	20.14	0.04	1.234
P11	BGP44	14.25	0.70	1.1	1.276	19.94	0.02	1.072
P12	N1270	13.00	0.65	1.2	1.164	18.23	0.02	1.419
		13.01	0.65	1.3	1.138	18.15	0.01	1.416
		13.01	0.65	1.5	1.145	18.17	0.02	1.416
P13	PER195	14.07	0.69	1.1	1.393	20.08	0.02	1.140
		14.08	0.69	1.1	1.370	20.01	0.01	1.138
P14	PER199	14.10	0.69	1.1	1.052	18.88	0.02	1.147
		14.10	0.69	1.1	1.012	18.73	0.01	1.146

Table 12 – continued

Our ID	Other ID	R_{20}	A_B	psf	$\log A_e$	$(\mu)_e$	rms	$\log D_n$
P15	CR28	14.12	0.70	1.2	1.097	19.04	0.03	1.140
P16	CR27	13.95	0.69	1.1	1.348	19.78	0.02	1.182
		13.96	0.69	1.1	1.370	19.85	0.03	1.179
P17	N1272	13.09	0.65	1.2	1.775	20.39	0.03	1.414
P18	N1273	13.27	0.70	1.2	1.258	18.83	0.02	1.362
P19	I1907	13.66	0.70	1.1	1.460	20.01	0.04	1.246
P20	BGP111	15.41	0.69	1.3	0.764	19.06	0.03	0.802
		15.41	0.69	1.2	0.900	19.59	0.02	0.799
P21	PER152	14.96	0.65	1.3	0.839	18.96	0.02	0.914
		14.96	0.65	1.2	0.884	19.12	0.01	0.914
P22	CR36	14.04	0.70	1.1	1.095	18.93	0.02	1.169
P23	N1278	13.07	0.70	1.1	1.660	20.00	0.01	1.441
		13.10	0.70	1.3	1.650	20.00	0.01	1.431
		13.10	0.70	1.4	1.673	20.06	0.01	1.432
P26	BGP59	14.15	0.70	1.1	0.788	17.85	0.01	1.146
		14.18	0.70	1.3	0.805	17.94	0.00	1.137
		14.16	0.70	1.4	0.823	18.00	0.00	1.141
P27	U02673	13.68	0.69	0.9	1.559	20.27	0.04	1.235
P28	N1281	13.55	0.70	0.9	1.169	18.82	0.01	1.281
P29	N1282	13.20	0.69	1.4	1.406	19.34	0.02	1.368
		13.19	0.69	1.1	1.409	19.34	0.02	1.371
P30	N1283	13.70	0.69	1.4	1.225	19.11	0.01	1.251
		13.71	0.69	1.2	1.218	19.10	0.01	1.248
P31	PER163	14.55	0.77	1.9	0.828	18.37	0.00	1.057
P33	BGP33	14.03	0.77	1.2	1.157	19.16	0.02	1.168
		14.00	0.77	1.4	1.151	19.11	0.02	1.176
P34	I0313	13.54	0.70	2.2	1.393	19.58	0.02	1.285
P36	N1293	13.45	0.84	2.1	1.279	19.03	0.01	1.331
P37	U02698	13.20	0.75	2.5	1.306	18.88	0.01	1.398
P38	U02717	13.55	0.85	2.5	1.436	19.68	0.01	1.306
P39	U02725	13.77	0.88	1.8	1.199	18.98	0.02	1.260
Cluster : Coma (A1656)								
D68	I3963	14.54	0.04	1.0	1.266	20.50	0.02	0.887
D69	I3959	14.04	0.04	1.0	1.074	19.27	0.01	1.065
D70	I3957	14.56	0.04	1.0	0.874	18.99	0.01	0.934
D104	N4875	14.39	0.04	1.3	0.803	18.51	0.01	0.998
D105	N4869	13.71	0.05	1.3	1.215	19.48	0.01	1.148
D122	N4894	14.78	0.05	1.2	0.993	19.72	0.01	0.852
		14.80	0.05	1.2	0.936	19.51	0.01	0.852
D124	N4876	14.12	0.05	1.3	0.972	18.99	0.03	1.044
D125	-	15.04	0.05	1.3	0.484	17.71	0.01	0.876
D126	-	15.32	0.05	1.3	0.955	20.07	0.03	0.702
D127	-	15.70	0.05	1.3	0.749	19.57	0.02	0.650
D128	-	15.40	0.05	1.3	0.680	18.96	0.02	0.754
D129	N4874	13.14	0.05	1.3	2.112	21.68	0.04	1.303
D130	N4872	14.20	0.05	1.3	0.809	18.33	0.01	1.050
D131	N4871	14.16	0.05	1.3	1.144	19.66	0.02	1.012
D132	-	15.30	0.05	1.3	0.905	19.85	0.01	0.727
D148	N4889	12.55	0.05	1.3	1.813	20.30	0.02	1.489
		12.55	0.05	1.2	1.808	20.30	0.02	1.489
D149	-	15.71	0.05	1.3	1.026	20.71	0.02	0.564
		15.72	0.05	1.2	0.994	20.61	0.02	0.561
D150	I4011	14.76	0.05	1.3	0.983	19.65	0.02	0.865
		14.77	0.05	1.2	0.992	19.69	0.02	0.861
D151	N4886	14.09	0.05	1.3	1.214	19.87	0.01	1.023
		14.11	0.05	1.2	1.219	19.92	0.01	1.019
D152	I3998	14.52	0.05	1.3	1.110	19.89	0.03	0.914
D154	-	15.55	0.05	1.3	1.319	21.72	0.01	0.488
D155	N4873	14.20	0.05	1.3	1.114	19.64	0.02	0.998
D157	-	15.08	0.05	1.3	0.862	19.44	0.00	0.802
Cluster : A2199								
A21-F113	-	15.45	0.00	1.3	0.617	18.74	0.00	0.750
A21-F114	-	15.11	0.00	1.3	0.567	18.15	0.00	0.849
A21-F121	A2199-S26	14.43	0.00	1.7	1.265	20.38	0.00	0.924
A21-F144	A2199-S30	14.74	0.00	1.2	0.599	17.93	0.01	0.934
		14.76	0.00	1.3	0.602	17.98	0.00	0.927
A21-F145	-	14.56	0.00	1.2	1.235	20.42	0.03	0.874
		14.60	0.00	1.3	1.182	20.28	0.02	0.866
A21-F146	A2199-S34	15.28	0.00	1.2	0.713	18.99	0.01	0.779
		15.30	0.00	1.3	0.696	18.93	0.01	0.779
A21-F164	N6166	13.41	0.00	1.2	2.184	22.16	0.05	1.191
		13.40	0.00	1.3	2.179	22.14	0.05	1.195
		13.36	0.00	1.7	2.218	22.20	0.05	1.216
A21-Z34A	A2199-Z34A	14.08	0.00	1.3	1.251	19.95	0.03	1.035
A21-Z34AC	-	14.59	0.00	1.3	0.775	18.55	0.01	0.953

Table 12 – *continued*

Our ID	Other ID	R_{20}	A_B	psf	$\log A_e$	$(\mu)_e$	rms	$\log D_n$
Cluster : A2634								
A26-F1201	A2634-D79	15.18	0.18	1.6	0.791	19.11	0.01	0.823
		15.17	0.18	2.5	0.803	19.16	0.01	0.819
A26-F121	A2634-D80	15.28	0.18	1.6	0.660	18.64	0.01	0.816
		15.29	0.18	2.5	0.676	18.72	0.02	0.811
A26-F1221	N7720	13.34	0.16	1.2	1.592	20.26	0.04	1.272
		13.34	0.16	1.6	1.568	20.17	0.05	1.273
A26-F1222	A2634-D76	14.62	0.16	1.3	0.788	18.59	0.02	0.963
		14.62	0.16	1.6	0.751	18.44	0.02	0.964
A26-F129	A2634-D74	14.58	0.16	1.3	1.040	19.58	0.00	0.942
		14.57	0.16	1.6	1.029	19.51	0.01	0.948
A26-F134	A2634-D55	14.25	0.16	1.2	1.112	19.51	0.02	1.031
		14.24	0.16	1.6	1.096	19.43	0.02	1.036
A26-F138	A2634-D58	14.28	0.14	1.2	1.210	19.89	0.03	1.008
A26-F139	A2634-D57	14.13	0.14	1.2	1.218	19.81	0.01	1.050

Table 13. Combined spectroscopic and photometric parameters. For each galaxy with both spectroscopic and photometric data, we tabulate : Type = morphological type assigned from CCD images or other source (E = elliptical, S0 = S0/lenticular, R = morphological reject – spiral, disk S0 etc. – Q = unclassified); cz = heliocentric recession velocity (kms^{-1}); N_σ = number of velocity dispersion measurements; σ = central velocity dispersion (kms^{-1} ; corrected to standard system, see text); ε_σ = poisson error on mean σ value, N_{Mg2} = number of Mg₂ measurements; Mg₂ = magnesium index (magnitudes; corrected to standard system); N_{D_n} = number of photometric observations; A_B = B-band absorption coefficient; $\log A_e$ = log effective diameter (arcsec); $\langle \mu \rangle_e$ = mean surface brightness within A_e ; $\log D_n$ = log R-band photometric D_n parameter (arcsec).

Our ID	Other ID	Type	cz	N_σ	$\log \sigma$	$\varepsilon_{\log \sigma}$	N_{Mg2}	Mg ₂	ε_{Mg2}	N_{D_n}	A_B	$\log A_e$	$\langle \mu \rangle_e$	$\log D_n$
Cluster : 7S21														
S01	N0079	E	5479	1	2.280	0.030	1	0.312	0.009	1	0.05	1.354	20.00	1.132
S02	N0085A	S0	6189	1	2.025	0.030	1	0.244	0.009	1	0.05	1.502	20.99	0.953
S03	N0083	E	6262	2	2.395	0.021	2	0.326	0.009	1	0.09	1.659	20.43	1.318
S04	N0080	E	5741	2	2.398	0.021	2	0.308	0.006	1	0.09	1.691	20.28	1.364
S05	I1548	S0	5775	1	2.165	0.030	1	0.202	0.009	1	0.09	0.992	18.91	1.072
S06	-	S0	5646	2	2.103	0.021	2	0.211	0.009	1	0.09	1.128	20.34	0.796
S07	CGCG457-008	S0	5926	1	2.053	0.030	1	0.259	0.009	1	0.11	1.128	19.47	1.055
Cluster : Pisces														
Z17005	-	E	4651	1	2.010	0.030	1	0.208	0.009	1	0.17	0.937	19.14	0.969
Z16012	-	R	17740	1	2.224	0.030	1	0.293	0.009	1	0.14	0.941	19.80	0.779
Z14028	CGCG501-070	E	4263	2	2.294	0.024	2	0.327	0.007	2	0.18	0.928	18.40	1.143
Z01034	CGCG501-077	E	5156	2	2.079	0.024	2	0.270	0.007	1	0.16	1.192	19.79	1.026
Z01036	I1618	S0	4730	1	1.948	0.040	1	0.226	0.012	2	0.16	1.247	20.19	0.965
Z01047	-	E	5493	1	2.110	0.030	1	0.288	0.009	1	0.17	0.839	18.66	0.991
Z01043	N0375	S0	5920	1	2.249	0.040	1	0.277	0.012	1	0.17	0.840	18.50	1.035
Z01027	N0379	S0	5502	2	2.355	0.024	2	0.300	0.007	3	0.17	1.542	19.89	1.376
Z01030	N0380	E	4440	5	2.470	0.015	5	0.341	0.004	3	0.17	1.319	18.94	1.387
Z01035	N0383	E	5093	5	2.449	0.015	5	0.311	0.005	2	0.17	1.789	20.27	1.485
Z01035C1	N0382	E	5250	4	2.299	0.017	4	0.276	0.005	2	0.17	1.086	18.90	1.188
Z01049	N0384	E	4266	3	2.410	0.021	3	0.314	0.006	3	0.17	1.190	18.88	1.282
Z01045	N0385	E	5016	3	2.294	0.019	3	0.293	0.007	4	0.17	1.396	19.68	1.257
Z01041	N0386	E	5560	2	2.102	0.024	2	0.254	0.007	2	0.17	1.075	19.40	1.036
Z01046	N0388	E	5464	2	2.130	0.024	2	0.257	0.007	2	0.18	0.881	18.67	1.039
Z01032	-	S0	4763	1	2.011	0.040	1	0.274	0.012	1	0.18	1.100	20.08	0.852
Z04050	N0392	E	4679	3	2.361	0.021	3	0.302	0.006	3	0.18	1.374	19.29	1.351
Z04049	N0394	S0	4388	3	2.257	0.021	3	0.270	0.006	3	0.18	1.052	18.76	1.184
Z04051	N0397	E	4988	1	2.083	0.030	1	0.261	0.009	3	0.18	1.016	19.28	1.000
Z01026	N0398	S0	4912	1	2.006	0.030	1	0.264	0.009	1	0.18	1.155	19.63	1.046
Z01073	CGCG501-102	E	5176	2	2.187	0.024	2	0.280	0.007	2	0.18	1.061	19.17	1.062
Z05052	N0410	E	5314	4	2.470	0.016	4	0.352	0.006	2	0.19	1.735	19.93	1.524
Z10020	CGCG501-126	S0	4852	1	1.919	0.030	1	0.230	0.009	1	0.20	1.134	20.08	0.879
Z02057	N0420	E	5026	2	2.258	0.024	2	0.249	0.007	4	0.16	1.531	19.88	1.336
Z05034	I1638	S0	4828	4	2.153	0.016	4	0.278	0.005	2	0.16	1.244	19.63	1.119
Z05044	I1648	S0	5541	1	2.083	0.030	1	0.269	0.009	1	0.17	1.116	19.47	1.050
Cluster : HMS0122+3305														
H01056	I1680	S0	4438	1	2.122	0.030	1	0.269	0.009	1	0.17	1.035	19.05	1.073
H01078	I1673	E	5090	1	2.268	0.030	1	0.277	0.009	1	0.13	0.856	18.14	1.139
H01051	CGCG502-043	E	5237	2	2.097	0.024	1	0.268	0.009	1	0.13	1.100	19.41	1.048
H01041	N0499	E	4395	2	2.405	0.024	1	0.329	0.009	1	0.17	1.545	19.44	1.481
H01044	N0501	E	5010	1	2.201	0.030	1	0.306	0.009	1	0.16	1.029	19.16	1.041
H01064	N0507	S0	4937	3	2.458	0.019	2	0.299	0.006	1	0.16	1.668	19.70	1.512
H01057	N0508	E	5517	2	2.343	0.024	1	0.312	0.009	1	0.16	1.445	19.96	1.224
H01022	N0528	E	4810	1	2.372	0.040	0	-	-	1	0.17	1.330	19.20	1.338
H04010	N0529	E	4796	2	2.363	0.024	1	0.297	0.009	1	0.15	1.424	19.14	1.448
Cluster : A0262														
A01071	N0705	R	4524	1	2.256	0.040	1	0.270	0.012	1	0.24	1.181	19.19	1.209
A19041	U01269	S0	3848	2	2.055	0.021	2	0.187	0.006	1	0.13	1.479	21.05	0.910
A01094	-	S0	14620	1	2.433	0.030	1	0.312	0.009	1	0.18	1.030	19.48	0.955
A01043	N0687	E	5106	2	2.353	0.024	2	0.301	0.007	1	0.21	1.478	19.41	1.420
A01076	-	E	4284	2	2.094	0.024	2	0.272	0.007	1	0.24	1.154	20.02	0.931
A01074	N0704	S0	4724	2	2.194	0.024	2	0.288	0.007	1	0.24	1.153	19.22	1.155
A01067	N0703	E	5580	1	2.341	0.030	1	0.313	0.009	1	0.24	1.361	19.69	1.233
A01069	N0708	E	4864	2	2.340	0.021	2	0.321	0.006	1	0.24	2.095	21.75	1.282
A01047	CGCG522-048	Q	4151	1	2.147	0.030	1	0.265	0.009	1	0.24	1.327	19.95	1.104
A09029	I0171	Q	5381	2	2.280	0.024	2	0.258	0.007	1	0.20	1.777	20.47	1.407
A02025	N0759	E	4639	2	2.406	0.024	2	0.255	0.007	1	0.20	1.543	19.85	1.363
A05096	CGCG522-089	E	5245	1	1.953	0.030	1	0.222	0.009	1	0.18	1.290	20.55	0.897

Table 13 – *continued***Cluster : A0347**

B02	U01837	E	6582	1	2.286	0.030	1	0.307	0.009	1	0.34	1.589	20.43	1.234
B03	U01841	E	6373	1	2.363	0.030	1	0.309	0.009	2	0.34	1.813	20.76	1.337
B03C	-	Q	6649	1	2.473	0.030	1	0.310	0.009	2	0.34	0.588	17.51	1.027
B06	U01859	E	5917	1	2.550	0.030	1	0.354	0.009	1	0.31	1.182	18.68	1.321
B07	CGCG538-065	S0	5301	1	2.308	0.030	1	0.314	0.009	1	0.39	1.200	19.20	1.203
B08	N909	E	4978	1	2.273	0.030	1	0.276	0.009	1	0.27	1.284	19.36	1.235
B09	N910	R	5237	2	2.391	0.021	2	0.339	0.006	1	0.27	2.025	21.66	1.227
B10	N911	S0	5766	1	2.400	0.030	1	0.328	0.009	1	0.27	1.206	18.81	1.312
B11	N912	E	4418	1	2.235	0.030	1	0.295	0.009	1	0.24	1.219	19.52	1.138
B16	CGCG539-042	E	4885	1	2.185	0.030	1	0.272	0.009	1	0.30	1.336	19.94	1.120

Cluster : J8

J07038	-	S0	10136	1	2.261	0.030	1	0.284	0.009	2	0.32	0.993	19.74	0.848
J09035	-	S0	11133	1	2.451	0.030	1	0.340	0.009	1	0.35	1.143	20.01	0.915
J08035	-	R	10099	1	1.910	0.030	1	0.182	0.009	2	0.33	1.124	20.49	0.722
J08036	EFAR-J8-K	E	9803	3	2.288	0.021	3	0.297	0.006	2	0.33	1.206	20.02	0.972
J01065	-	S0	9103	1	2.125	0.030	1	0.168	0.009	2	0.28	0.843	18.95	0.913
J01067	EFAR-J8-I	E	9237	2	2.300	0.024	2	0.315	0.007	1	0.28	1.205	20.18	0.920
J01060	I1803	E	9583	1	2.565	0.030	1	0.352	0.009	1	0.28	1.278	19.22	1.273
J01070	I1806	E	10219	3	2.332	0.021	3	0.316	0.006	2	0.31	1.295	20.21	1.004
J03049	-	E	9933	2	2.400	0.024	2	0.275	0.007	2	0.28	1.438	20.51	1.062
J01055	-	E	9616	2	2.184	0.021	2	0.294	0.006	3	0.28	1.915	22.30	0.831
J01056	CGCG483-068	E	9513	3	2.371	0.019	3	0.333	0.006	3	0.31	1.695	21.23	1.055
J01049	CGCG483-070	E	8562	3	2.494	0.021	3	0.322	0.006	1	0.31	1.164	19.32	1.136
J01069	I1807	E	9058	2	2.309	0.024	2	0.279	0.007	1	0.31	1.118	19.44	1.062
J01080	-	S0	9731	1	2.216	0.030	1	0.255	0.009	1	0.34	0.869	19.28	0.855

Cluster : Perseus (A0426)

P01	I0293	E	4714	1	2.171	0.040	1	0.274	0.012	1	0.56	1.597	20.76	1.114
P02	N1224	S0	5235	1	2.384	0.030	1	0.274	0.009	1	0.56	1.455	19.71	1.322
P03	I0310	S0	5660	1	2.329	0.030	1	0.253	0.009	1	0.60	1.628	20.06	1.377
P05	I0312	S0	4988	1	2.342	0.040	1	0.310	0.012	1	0.76	1.399	19.58	1.310
P07	CR19	E	3544	1	2.081	0.030	1	0.243	0.009	1	0.65	1.336	20.61	0.912
P08	CR20	E	6461	2	2.294	0.021	2	0.269	0.006	1	0.65	1.482	20.14	1.234
P11	BGP44	E	4247	1	2.192	0.030	1	0.279	0.009	1	0.70	1.276	19.94	1.072
P12	N1270	E	4997	2	2.530	0.024	2	0.361	0.007	3	0.65	1.149	18.18	1.417
P13	PER195	E	8396	2	2.231	0.024	2	0.286	0.007	2	0.69	1.382	20.05	1.139
P14	PER199	S0	5102	3	2.323	0.019	3	0.289	0.006	2	0.69	1.032	18.81	1.147
P15	CR28	E	6213	1	2.317	0.030	1	0.292	0.009	1	0.70	1.097	19.04	1.140
P16	CR27	S0	8063	1	2.228	0.040	1	0.280	0.012	2	0.69	1.359	19.82	1.180
P17	N1272	S0	3801	7	2.417	0.013	6	0.346	0.004	1	0.65	1.775	20.39	1.414
P18	N1273	S0	5397	1	2.311	0.040	1	0.263	0.012	1	0.70	1.258	18.83	1.362
P19	I1907	S0	4489	1	2.285	0.040	1	0.292	0.012	1	0.70	1.460	20.01	1.246
P20	BGP111	E	3963	1	1.925	0.030	1	0.283	0.009	2	0.69	0.832	19.33	0.801
P21	PER152	E	3940	2	2.134	0.021	2	0.316	0.006	2	0.65	0.861	19.04	0.914
P22	CR36	E	7470	1	2.301	0.040	1	0.294	0.012	1	0.70	1.095	18.93	1.169
P23	N1278	E	6064	3	2.410	0.021	2	0.309	0.007	3	0.70	1.661	20.02	1.435
P26	BGP59	E	5315	1	2.307	0.030	1	0.287	0.009	3	0.70	0.805	17.93	1.141
P27	U02673	E	4434	1	2.290	0.040	1	0.302	0.012	1	0.69	1.559	20.27	1.235
P28	N1281	E	4300	1	2.432	0.030	1	0.328	0.009	1	0.70	1.169	18.82	1.281
P29	N1282	E	2223	4	2.325	0.017	4	0.290	0.005	2	0.69	1.408	19.34	1.370
P30	N1283	E	6746	2	2.320	0.028	1	0.291	0.012	2	0.69	1.222	19.11	1.249
P31	PER163	E	5481	2	2.249	0.021	2	0.290	0.006	1	0.77	0.828	18.37	1.057
P33	BGP33	S0	4950	1	2.216	0.030	1	0.293	0.009	2	0.77	1.154	19.13	1.172
P34	I0313	S0	4432	1	2.375	0.030	1	0.335	0.009	1	0.70	1.393	19.58	1.285
P36	N1293	E	4167	3	2.321	0.021	3	0.318	0.006	1	0.84	1.279	19.03	1.331
P37	U02698	E	6451	2	2.557	0.024	2	0.340	0.007	1	0.75	1.306	18.88	1.398
P38	U02717	E	3793	2	2.189	0.024	2	0.239	0.007	1	0.85	1.436	19.68	1.306
P39	U02725	S0	6215	1	2.333	0.030	1	0.297	0.009	1	0.88	1.199	18.98	1.260

Cluster : A2199

A21-F113	-	Q	8052	4	2.217	0.015	4	0.269	0.004	1	0.00	0.617	18.74	0.750
A21-F114	-	S0	9184	4	2.297	0.015	4	0.303	0.004	1	0.00	0.567	18.15	0.849
A21-F121	A2199-S26	E	8768	2	2.239	0.021	2	0.287	0.006	1	0.00	1.265	20.38	0.924
A21-F144	A2199-S30	E	8524	2	2.411	0.021	2	0.262	0.006	2	0.00	0.601	17.95	0.931
A21-F145	-	R	7610	2	2.173	0.021	2	0.289	0.006	2	0.00	1.209	20.35	0.870
A21-F146	A2199-S34	E	8314	2	2.205	0.021	2	0.272	0.006	2	0.00	0.704	18.96	0.779
A21-F164	N6166	E	9348	2	2.442	0.021	2	0.323	0.006	3	0.00	2.194	22.17	1.201
A21-Z34A	A2199-Z34A	E	8721	2	2.298	0.021	2	0.288	0.006	1	0.00	1.251	19.95	1.035
A21-Z34AC	-	S0	8964	2	2.337	0.021	2	0.324	0.006	1	0.00	0.775	18.55	0.953

Table 13 – *continued*

Cluster : A2634

A26-F138	A2634-D58	E	10872	4	2.343	0.017	4	0.316	0.005	1	0.14	1.210	19.89	1.008
A26-F139	A2634-D57	E	9591	4	2.331	0.017	4	0.327	0.005	1	0.14	1.218	19.81	1.050
A26-F129	A2634-D74	S0	8425	3	2.315	0.019	3	0.301	0.006	2	0.16	1.035	19.55	0.945
A26-F121	A2634-D80	E	9582	4	2.262	0.017	4	0.286	0.005	2	0.18	0.668	18.68	0.814
A26-F1201	A2634-D79	S0	10166	4	2.234	0.019	4	0.295	0.005	2	0.18	0.797	19.13	0.821
A26-F134	A2634-D55	E	9288	3	2.342	0.019	3	0.300	0.006	2	0.16	1.104	19.47	1.034
A26-F129	A2634-D74	S0	8425	3	2.315	0.019	3	0.301	0.006	2	0.16	1.035	19.55	0.945
A26-F1221	N7720	E	9104	5	2.527	0.015	5	0.331	0.004	2	0.16	1.580	20.22	1.273
A26-F1222	A2634-D76	E	8123	5	2.320	0.015	5	0.296	0.004	2	0.16	0.770	18.52	0.964
A26-F139	A2634-D57	E	9591	4	2.331	0.017	4	0.327	0.005	1	0.14	1.218	19.81	1.050